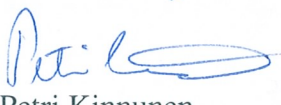# ANTIOXI - Development and testing of an integrated corrosion and activity build-up model

Authors	Iva Betova, Martin Bojinov, Petri Kinnunen, Timo Saario
Confidentiality	Public

Report's title	
ANTIOXI - Development and testing of an integrated corrosion and activity build-up model	
Customer, contact person, address	Order reference
EC / Marc Deffrennes, Commission européenne, Rue du Champ de Mars 21, B- 1050 Brussels, Belgium	
Project name	Project number/Short name
ANTIOXI	6402 ANTIOXI
Author(s)	Pages
Iva Betova, Martin Bojinov, Petri Kinnunen, Timo Saario	47/
Keywords	Report identification code
stainless steel, nickel alloy, oxidation, high-temperature water, activity incorporation, modelling	VTT-R-10525-08

Summary

An integrated deterministic model for corrosion and activity incorporation in oxides on structural materials in nuclear power plant coolant circuits is proposed based on fundamental physico-chemical mechanisms. In order to ensure adequate modelling, uncertain or non-determined fundamental parameters are set or adjusted within the range of reasonable values by evaluating well-defined or well-controlled in-plant observations or laboratory experiments. As a result of the calculation procedure developed on the basis of the model, the kinetic and transport parameters of the growth and restructuring of the oxides on austenitic stainless steels (AISI 304, 0X18H10T and AISI 316) and nickel based alloys (Alloys 600 and 690) in Light Water Reactors (LWRs) were determined via quantitative comparison of the equations of the Mixed-Conduction Model for oxide films with ex-situ analytical results on thickness and composition of such layers obtained from both laboratory and in-reactor exposures. The obtained parameters were used to predict general corrosion of stainless alloys in terms of oxide film growth and restructuring, as well as corrosion release in several specific cases covering all the three types of LWRs – Boiling Water Reactors (BWRs), Pressurised Water Reactors (PWRs) and Water-Water Energy Reactors (WWERs). Kinetic and transport parameters for the incorporation of Co and Zn in the oxide layers on stainless steels and nickel alloys are also estimated by reproducing the experimental depth profiles of these elements. The diffusion-migration equations for the non-steady state transport of such species were solved subject to the boundary conditions at the solution side set by the stability constants of the corresponding Zn and Co complexes. The calculatory results are discussed in terms of the influence of incorporation of solution-originating species on the kinetics of film growth and layer restructuring.

Confidentiality	Public

Espoo, 8.12.2008
Signatures

Liisa Heikinheimo
Technology Manager

Petri Kinnunen
Senior Research Scientist

Distribution (customer and VTT)
European Commission, 1 original
VTT, 1 original

Preface

The work discussed in the present report has been carried out as in the Work Packages 1,2 and 4 of the project FP6-036367 A deterministic model for corrosion and activity incorporation in nuclear power plants (ANTIOXI) in 2006 - 2007. The ANTIOXI project is a part of the EURATOM FP6 Programme "Advanced tools for nuclear safety assessment and component design".

The ANTIOXI project in EURATOM FP6 concentrates on development of modelling tools for activity incorporation and corrosion phenomena into oxide films on construction materials in light water reactor environments. In the present report, the integrated deterministic model for corrosion and activity incorporation is described in detail and the specific cases predicted by the model calculations are discussed in terms of oxide growth, restructuring and incorporation of coolant-originating species.

Espoo, 19.12.2008

Authors

Contents

1 Introduction

1.1 Definition of the target

The two main issues in having a safe and economic operation of a nuclear power plant are to minimise the risk and occurrence of stress corrosion cracking, and to minimise the exposure of the staff and other people to ionising radiation. Although these two issues are very disparate phenomena, the common and most important factor for both of them is the integrity of the oxide films on the structural materials in the nuclear power plants.

All materials used in the nuclear power plants rely on a passivating oxide film. This means that the oxide film formed from the corrosion attack of water on the material will protect the underlying material against further attack. The material in itself would, according to the thermodynamics, decompose into a mixture of metal oxides without this protective layer. This deterioration of the material is also observed if the passivating film is destroyed for a certain reason. The protective effect of the oxide layer originates from a low solubility of the oxide itself and a slow reaction rate for any chemical interaction between the oxide film and the surrounding environment, the coolant water in light water reactors (LWRs). The protective effect is, however, never perfect. This means that corrosion of the base material is always occurring to some extent. Furthermore, changes in the chemical composition or pH of the surrounding water, or an increase in temperature, could increase the reaction rate and hence diminish the protective ability of the oxide film.

During the long-term commercial use of LWRs, a huge experience has been gained about the materials behaviour in addition to the basic mechanical properties. Yet, the increasingly faster change of the environmental conditions has made it difficult to test all possible combinations of materials and environments in order to assess the long-term behaviour of the materials, or rather the behaviour of the protective oxides on the materials, in these new combinations of environments. The corrosion behaviour of a certain material is always depending on the environment, which influences the release of corrosion products from the already existing oxide surfaces. The behaviour of oxide films in the primary system of a nuclear power plant is hence a complex function of their behaviour in coupled localised areas of the system depending on each other and all local environmental factors. The inference is that a full assessment of the materials behaviour in LWRs cannot be gained only through materials testing in simulated or even real LWR environments, since the oxide film stability and protectiveness will depend on a large number of factors, and so will the materials integrity. We need a more fundamental understanding for each kind of oxide film and the impact of environmental factors on the film behaviour. We also need a theory or a modelling tool that can take into account the interaction between the various local oxides with their local chemistry in order to have an integral description and understanding of the stress corrosion cracking and the activity build-up in any LWR.

1.2 Oxide film growth, restructuring and activity incorporation

The activity build-up in nuclear power plants is influenced by the oxide films in several ways. To have activity build-up a certain corrosion release from the materials is needed to allow corrosion products to deposit in the core region and become activated. Without corrosion products from the non-core structural materials, basically only the cladding and its oxide would be the source for any activity distribution. The oxide formed on the zirconium material,

does, however, almost exclusively consist of zirconium oxide, which has a very low solubility in BWR conditions and also markedly low solubility in PWR and WWER environments. This means that without deposited corrosion products in the core, the activity release would be almost exclusively due to flaking of oxide on fuel cladding. The activation products of zirconium, i.e. Zr-95 and Nb-95 and their derivatives, have short half-life (e.g. 64 days for Zr-95) and the activation build-up problem would be virtually non-existent in LWRs.

In reality, the materials in the LWR primary systems do release a significant amount of products to the coolant through corrosion. Flow assisted corrosion enhances the corrosion release from some parts of the system and hence provides even higher contributions to the primary coolant flow. The corrosion release in itself will affect the oxide film build-up of any materials downstream the releasing material.

The neutron activation of the core crud will depend on the amount of crud and the residence time for the deposit on the core. These aspects are indirectly related to the integral corrosion release from all the materials in contact with the coolant before the core passage. The activity released from the core is then partly in form of transmuted corrosion products, but still to a large extent the transmuted nuclides are of the same or similar elements, i.e. cobalt (Co-58 and Co-60), iron (Fe-59), manganese (Mn-54), zinc (Zn-65), and chromium (Cr-51). Still, most of the released core crud will be non-transmuted, and hence the core will be a sink and source for the corrosion products being distributed by the coolant. The activated corrosion products will, however, be responsible for any activity build-up.

The activity build-up in the nuclear power plant is either resulting from particulate matter mainly depositing in low flow locations, or, which is one of the main focus points in this review and the planned model development, resulting from incorporation of dissolved corrosion products with the oxide films in contact with the coolant carrying the ionic activity. The ionic activity can interact with the oxide film and be incorporated, all as a function of the oxide growth, release, and restructuring behaviour.

1.3 Oxide films, localised corrosion and stress corrosion cracking

The protective ability of the oxide film is hindering general corrosion of the base alloy and hence the passive film assures that no significant component thinning is occurring during the exposure to the surrounding coolant in the LWR. Even very small localised attacks on the oxide film could, however, be detrimental for the component. Although the localised attack would only affect a small area or part of the material, it could still be threatening the safe operation of the LWR through stress corrosion cracking (SCC). The passive behaviour of the oxide film could then be important in two ways.

The first is for the localised corrosion attack itself. To have SCC, in addition to a tensile stress applied to the material, the material must be susceptible to localised attack, e.g. sensitised, and there must be an aggressive environment causing the attack. Although the actual chemistry is rather different in Boiling Water Reactors (BWRs) compared to Pressurized Water Reactors (PWRs) or Water-Water Energy Reactors (WWERs), still the same factors are needed. If the stressed oxide film is prone to localised attacks via chemical interaction with the coolant water, so called pitting could develop on the material surface. The pits, formed where the oxide film is locally the least protective, will establish a local aggressive chemistry in the bottom of the pit. The weakest spots of the oxide film will hence be the locations where further attacks to the underlying alloy occur. When a certain depth, normally claimed to be

approximately 20 µm or slightly deeper, has been penetrated in the base alloy, the pit or incipient attack can develop into a propagating crack if sufficient stress is applied. The weakest spot in the oxide film is thus transformed into the weakest spot for cracking of the materials.

The second aspect is the re-passivation kinetics, i.e. the ability to quickly reform a protective passive layer, which is also important for the development of SCC. If the material does not re-passivate, the localised attack would be more extended and actually open up the attack area to allow wash-out of the local chemistry. The re-passivation hence allows for the slightly less stressed areas of exposed metal to rebuild an oxide which will protect them against further attack, confining the attack to a small area. This forces the attack to grow into the material instead of extending laterally and stabilising the local chemistry in a more and more confined location. In this way the localised attack continues to penetrate the material and keeps the intergranular or transgranular crack growing by continuously re-establishing the aggressive chemical conditions until the crack has propagated through the material.

The re-passivation kinetics is always important what comes to SCC in LWR environments. The weak spots in the film are only important when the tensile stresses do not immediately crack the brittle oxide film but a localised chemical attack is needed to start the cracking behaviour. Just as for the general corrosion and the impact of the environment on the passivation behaviour in general, the environment will be of decisive importance what comes to the localised attack and the re-passivation kinetics.

2   Goal

The main objective of the present report is to describe the development of a theoretical predictive model of the oxide film behaviour on structural materials in nuclear power plants in relation to activity build-up and corrosion phenomena. This model comprises of three parts: a quantitative treatment of the growth of the inner, or barrier oxide film layer via solid state transport of matter and charge mediated by the generation, diffusion-migration and consumption of point defects (interstitial ions and vacancies), a diffusion formalism for the growth of the crystallites of the outer (porous) layers and an adsorption/surface complexation model for the processes at the coolant/oxide interface. The model is developed into a quantitative procedure for the estimation of kinetic, structural and transport parameters and is compared with experimental data for a range of specific cases covering all the three types of LWRs –BWRs, PWRs and WWERs.

3   Description

The typical compositions of the structural materials, the oxidation mechanism of which is subject to discussion in the present report, are summarized in Table 1 (stainless steels) and Table 2 (nickel-based alloys).

Table 1. Composition of stainless steels (weight-%).

Material	C	Cr	Cu	Fe	Mn	Ni	S	Si	Mo	Other
AISI 304	0.08	19	n.q.	bal.	2	9.3	0.03	1	n.q.	N : 0.1
0X18H10T (AISI 321)	0.05	18	0.15	bal.	2	10.4	0.03	0.8	n.q.	Ti: 0.47 Co:0.15
AISI 316L(NG)	0.015	16.5	0.26	bal.	1.73	10.5	0.002	0.54	2.55	N : 0.056
AISI 316L	0.03	17	n.q.	bal.	2	12	0.03	1	2.5	N:0.1

Table 2. Compositions of nickel-based alloys (weight-%).

Material	C	Cr	Cu	Fe	Mn	Ni	S	Si
Alloy 600	<0.15	16	≤0.5	8	≤1.0	bal.	0.015	≤0.5
Alloy 690	<0.05	30	≤0.5	9	0.31	bal.	0.006	≤0.5

The basic limitation for the oxide film growth rate on stainless steels and nickel-based alloys and hence the oxide thickness is the solid state transport rate within the inner, also called barrier, oxide film layer. Models for such transport have been developed for many years, but only recently has the modelling reached a sufficient sophistication to allow a reasonably good quantitative correlation between the modelled values and the growth rates of oxide films on structural materials in real LWR environments. Such a quantitative model, called the Mixed-Conduction Model (MCM) is described to some detail in the Theory section of the report. Also the evolution of the micro- and nanostructure of the inner oxide layer(s) and its influence on the mechanism(s) of ion transport in that layer is taken into account in a quantitative way. In the Theory section, an approach to the growth of the outer and deposited layer crystallites using diffusion formalism is also presented, and the coupling between the models for the compact and porous layers is discussed. In order to treat the incorporation of coolant-originating species, this model has to be coupled to an adsorption-surface complexation approach which is briefly described in the Theory section as well. The associated calculation procedure that enables the estimation of the kinetic and transport parameters using a quantitative comparison of the model equations with experimental data stemming mainly from surface and in-depth characterisation of the oxide films on structural materials by ex-situ analytical techniques is also outlined. The physical significance and the relevance of the parameter estimates is described at length in the subsequent section, in which a systematic review of the calculatory results for oxide films formed both in laboratory and during plant operation is presented. Finally, the limitations of the proposed integrated model are summarized and some trends for future research in the field are proposed.

4 Limitations

Since our goal is to compare the predictions of the proposed model with depth profiles of metallic constituents of the oxides, which are available in the literature for a large range of specific cases pertinent to LWRs, we do not distinguish between the defects via which respective metallic constituent is transported through the inner layer of oxide. In the absence of representative information on the pore diameter and tortuousity of the outer and deposited layers of oxide, and also of reliable data on the crystallite size of such layers, their growth is formally treated as a diffusion process in a matrix constituted of the outer layer crystals and

the electrolyte in between, which precludes at this stage the precise determination of the kinetic and transport parameters of all the elementary steps involved in the outer layer growth.

5   Theory

5.1   The Mixed-Conduction Model

The MCM is at the conceptual level quite similar to the Point Defect Model (PDM) proposed and developed by Macdonald and co-workers during the last three decades [1-4]. However, some basic assumptions made in these models differ to a certain extent. Thus it is worth summarising the assumptions made within the frames of the MCM:

1. The film consists mainly of oxide and the amount of hydroxide in the film is negligible. Thus the possible doping of the layer with incorporated hydrogen e.g. playing the role of electron donor is not taken into account. The stoichiometric composition of the oxide varies gradually with potential without abrupt structural changes.
2. Possible ionic charge carriers in the film are anion, i.e. oxygen, vacancies, interstitial cations and cation vacancies.
3. A certain concentration of oxygen vacancies is maintained in the film, in order to explain the growth of the film via the inward-motion of oxygen ions.
4. The electric field strength in the film is assumed to be homogeneous and independent of potential, while the film thickness is assumed to be proportional to the applied potential. However, very recent thickness measurements indicate that the latter assumption may not be fulfilled at high temperatures.
5. For the transport of ionic species, the high-field approximation is used at room temperature and the low-field approximation at high temperatures, i.e. the electric field strength is assumed to decrease as the film becomes thicker and/or more defective at high temperatures.
6. An exponential dependence on the local potential drops is assumed at both interfaces for the interfacial rate constants. However, the potential drop at the alloy/oxide interface is supposed to be independent on the applied potential, which is in turn distributed between the oxide bulk and the oxide/electrolyte interface. In other words, the rates of the reactions at the alloy/oxide interface are not adjusted by the applied potential but rather by the transport of defects through the oxide.
7. Each ionic point defect in the film plays the role of an electron donor or acceptor. This means that it is accompanied by an electronic defect that contributes to the electronic conductivity in the film.

In the MCM the impedance of the metal/film/solution system is a combination of the impedances of the interfaces and that of the bulk film. For the passive film in the steady state the interfacial impedances can be usually neglected, because the reactions at the interfaces are either very fast compared with the transport in the oxide film, or the capacitances corresponding to these reactions are very large so that the impedances are not distinguishable. The film impedance consists of the electronic and ionic contributions. Using the general transport equations given by Fromhold and Cook [5] and defining the appropriate boundary conditions, the concentration profiles for different ionic charge carriers in the film can be defined. Further, the electronic conductivity is proportional to the concentration of defects, and equations describing the electronic conductivity can be derived for both low and high potentials according to the type of charge carriers having the strongest effect. The transfer

function for the electronic contribution to the total conductivity and to the film impedance depending on the film thickness and potential can be derived from an explicit physico-chemical model, being mathematically equivalent to the formal model of Young [6] for insulating layers with defect induced conductivity. This makes the bridge to the chemiconductor model at the conceptual level [7]. The ionic part of the film impedance, on the other hand, often reduces to a resistance, if the apparent diffusion coefficient is high, or to a Warburg impedance in the case of a low diffusion coefficient.

The MCM has been successfully used previously to explain the features of several metals and alloys in the passive region at room temperature [8-11]. A comprehensive description of the model for structural materials in high temperature aqueous electrolytes such as LWR coolants is given below.

Taking into account the above assumptions, the basic kinetic scheme of the MCM is shown in Fig. 1 for the passive film on Fe as an example.
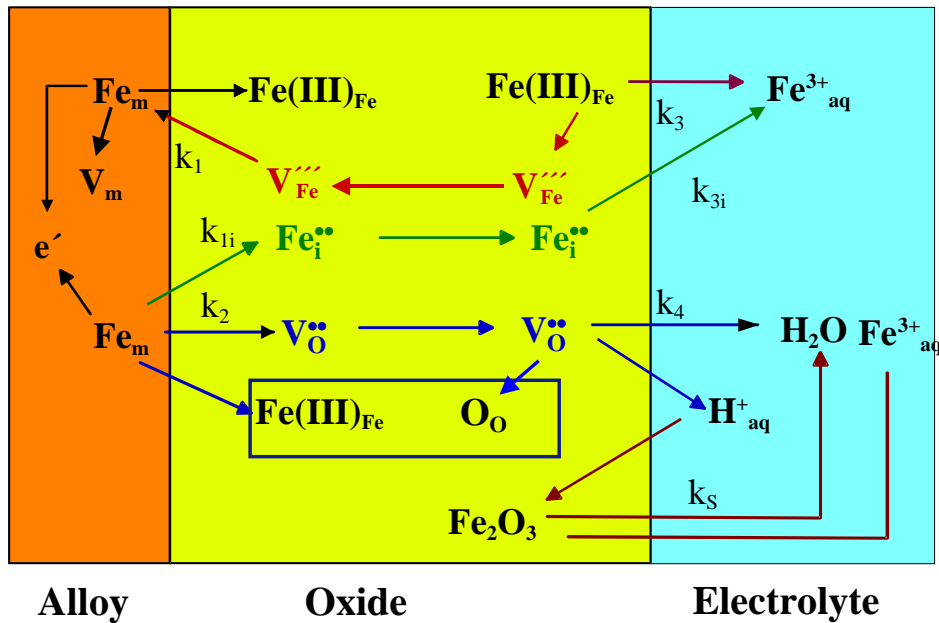

Fig. 1. Basic kinetic scheme of the MCM illustrated for the passive film on iron.

As stated above (assumption 5) because of the increase of their defectiveness, the films at high temperature are not likely to support the high-field conditions. Thus the steady-state solutions of the generalised transport equation given by Fromhold and Cook [5] with a low-field approximation results in equations of the type

$$J_O(x) = -D_O \frac{\partial c_O(x)}{\partial x} - \frac{D_O}{a} c_O(x) \left[\frac{zFa\vec{E}(x)}{RT} \right] \qquad (1)$$

These equations together have to be solved with the appropriate boundary conditions in order to calculate the profiles of defects within the film. In this case, the steady state concentration profiles of anion and cation vacancies, as well as interstitial cations, can be written as follows:

$$c_O(x) = \chi k_2 \left[\left(\frac{1}{k_4} - \frac{1}{2KD_O} \right) e^{-2Kx} + \frac{1}{2KD_O} \right]$$

$$c_M(x) = k_3 \left[\left(\frac{1}{k_1} - \frac{1}{2KD_M} \right) e^{-3K(L-x)} + \frac{1}{3KD_M} \right] \qquad (2)$$

$$c_i(x) = k_{1i} \left[\left(\frac{1}{k_{3i}} - \frac{1}{2KD_i} \right) e^{-2Kx} + \frac{1}{2KD_i} \right]$$

where $K = F\vec{E}/RT$. For a detailed explanation of the symbols used, the reader is referred to the Nomenclature section.

The obtained expressions for the concentration profiles of positive (e.g. oxygen vacancies) and negative (e.g. cation vacancies) defects are illustrated in Fig. 2. They contain exponential terms that depend on the distance within the film and the applied potential. The latter dependence is included in the dependence of the interfacial rate constants on potential. This means that, according to the model, the difference between the distribution of defects in films formed at room and at a high temperature is only quantitative.
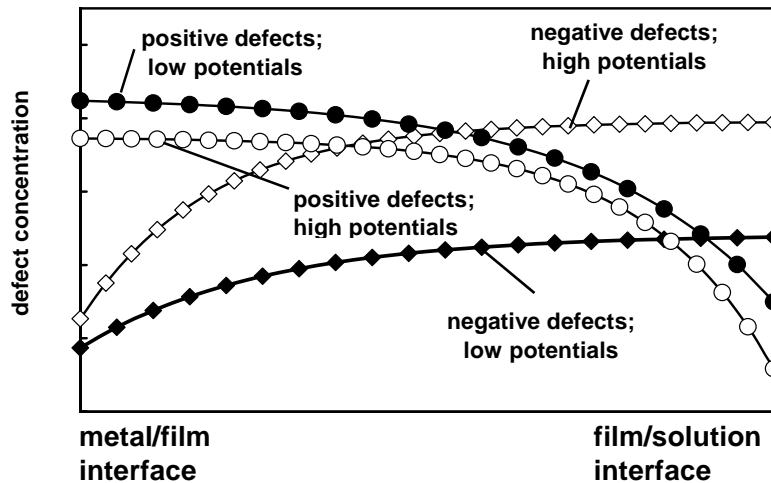

Fig. 2. A scheme of simulated profiles of defect concentrations through the oxide film at high and at low potentials.

5.2 Inner layer growth according to the proposed approximation of the MCM

According to the MCM [8-17], the inner layer growth proceeds via the sequence of reactions involving the generation of normal cation positions and injection of oxygen vacancies at the alloy/film interface, their transport via a diffusion-migration mechanism and subsequent consumption at the film/electrolyte interface via a reaction with adsorbed water. In parallel to that process, metal cation dissolution through the film, involving either the generation of cation vacancies at the outer interface, their transport and consumption at the inner interface, or generation, transport and release of interstitial cations, respectively, is also expected to occur. Due to the low solubility of the constituent metals in the high-temperature electrolyte, the dissolved cations are mainly re-deposited to form the outer layer. Such a situation is illustrated schematically in Fig. 3 for film growth on stainless steel. In this figure, the oxidation and dissolution of nickel has been omitted for the sake of simplicity. As will be

pointed out later in this report, in addition to the inner and outer oxide layers resulting from the release of cations from the oxide, also a deposited layer formed via adsorption of solution originating particles onto the oxide surface can exist.

The goal of the present work is to elaborate a calculatory procedure for the determination of kinetic and transport parameters of individual alloy constituents. Such a procedure is intended to be validated by comparing the predictions of the model with experimentally measured depth profiles of oxide constituents, normalised to its total cation content to exclude the influence of the oxygen profile. In order to reduce the number of variables, we intend to use a simplified approach scheme presented in Fig. 4. Although it has been presumed that Cr and Ni are transported through the oxide via vacancies and Fe via interstitial cation sites, at this point we do not distinguish between the types of the defects via which the respective metallic constituent is transported through the inner layer of oxide. Thus e.g. the reaction rate constant at the alloy/inner layer interface for Fe (k_{1Fe}) can be regarded as a sum of the reaction rate constants of oxidation of Fe producing Fe interstitials (k_{1iFe}), producing normal Fe positions and oxygen vacancies (k_{2Fe}) and consuming cation vacancies with the simultaneous production of normal Fe positions (k_{1FeM}), the same being the case for Cr and Ni and also for the inner layer/electrolyte interface in the pores of the outer layer. On the other hand, the diffusion coefficients D_{Cr}, D_{Fe} and D_{Ni} can be regarded as characterising the overall transport of cations through the inner layer resulting either from its growth via generation, transport and consumption of oxygen vacancies or the dissolution of these cations through the inner layer via a vacancy or interstitial mechanism.
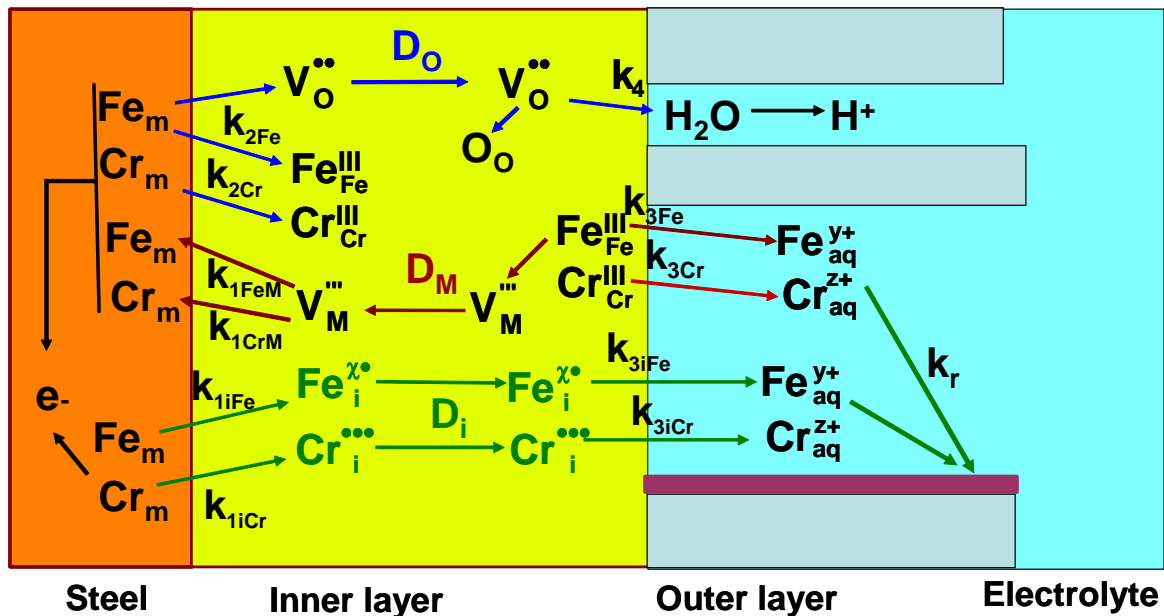

Fig. 3 *A scheme of the growth of the inner layer, dissolution of cations through it and subsequent precipitation of the outer layer of the corrosion film on stainless steel according to the MCM.*
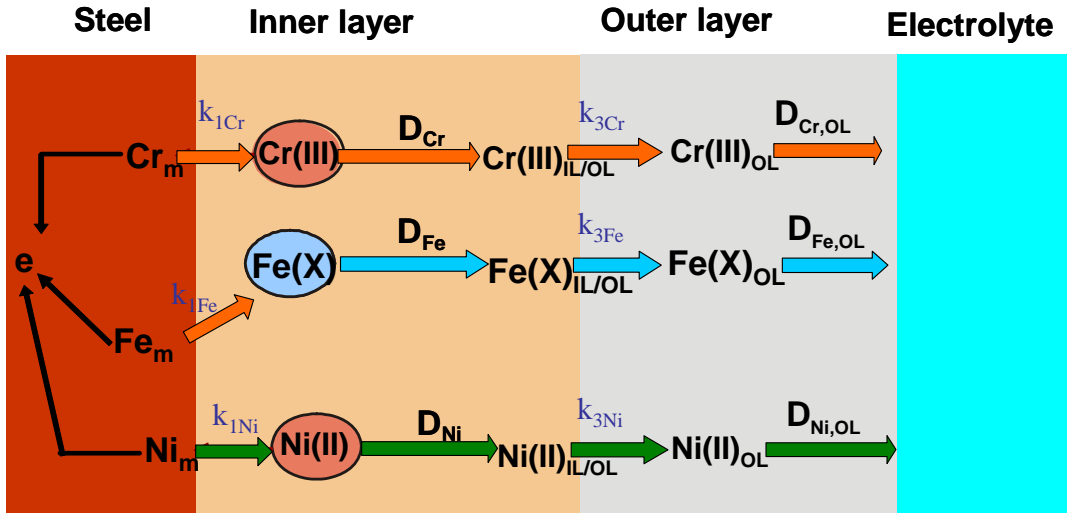
Fig. 4 *A simplified scheme of the growth of the inner and outer layers of the film formed on a structural material according to the proposed simplified approach. For details see text.*

Mathematically, we treat the problem in conceptual analogy to the approach presented in Ref 18, where the depth profile of W in a binary Ni-W alloy has been calculated on the basis of the PDM. The depth profile of a metallic oxide constituent j = Fe, Cr, Ni, etc., can be expressed as the dependence of its molar fraction, $y_j = c_j V_{m,MO}$, on the distance within the inner layer, where c_j is its molar concentration and $V_{m,MO}$ the molar volume of the phase in the layer. Respectively the transient diffusion-migration equations for each component read as

$$\frac{\partial y_{Fe}}{\partial t} = D_{Fe} \frac{\partial^2 y_{Fe}}{\partial x^2} + \frac{XF\vec{E}D_{Fe}}{RT} \frac{\partial y_{Fe}}{\partial x}$$

$$\frac{\partial y_{Cr}}{\partial t} = D_{Cr} \frac{\partial^2 y_{Cr}}{\partial x^2} + \frac{3F\vec{E}D_{Cr}}{RT} \frac{\partial y_{Cr}}{\partial x} \qquad (3)$$

$$\frac{\partial y_{Ni}}{\partial t} = D_{Ni} \frac{\partial^2 y_{Ni}}{\partial x^2} + \frac{2F\vec{E}D_{Ni}}{RT} \frac{\partial y_{Ni}}{\partial x}$$

where X stands for the nominal valency of Fe in the oxide, which is close to 2.67 in the passive region and close to 3 in the transpassive region. The boundary conditions at the alloy/film and film/electrolyte interfaces, as well as the initial conditions can be written as

$$y_{Fe}(x,0) = y_{Fe,a}, \, y_{Cr}(x,0) = y_{Cr,a}, \, y_{Ni}(x,0) = y_{Ni,a}$$

$$y_{Fe}(0,t) = y_{Fe,a}, \, y_{Cr}(0,t) = y_{Cr,a}, \, y_{Ni}(0,t) = y_{Ni,a}$$

$$y_{Fe}(L_i,t) = \frac{k_{1Fe} y_{Fe,a}}{V_{m,MO}} \left[\frac{1}{k_{3Fe}} + \frac{RT}{XF\vec{E}D_{Fe}} \right] \qquad (4)$$

$$y_{Ni}(L_i,t) = \frac{k_{1Ni} y_{Ni,a}}{V_{m,MO}} \left[\frac{1}{k_{3Ni}} + \frac{RT}{2F\vec{E}D_{Ni}} \right]$$

$$y_{Cr}(L_i,t) = \frac{k_{1Cr} y_{Cr,a}}{V_{m,MO}} \left[\frac{1}{k_{3Cr}} + \frac{RT}{3F\vec{E}D_{Cr}} \right]$$

where $x = 0$ at the alloy/film interface and $x = L_i$ is the film/coolant or inner layer/outer layer interface, L_i being the inner layer thickness.

At this stage of the modelling, we do not consider the existence of a transition layer between the bulk alloy and the alloy/oxide interface in which the composition of the underlying alloy is modified. In other words, the respective mass fractions at the alloy / film interface are taken as equal to the fractions in the bulk alloy. Albeit admittedly a crude simplification, this assumption facilitates the computations markedly. The introduction of the transition layer at a later stage of this work is, however, conceptually straightforward. Another simplification introduced at this point is that at *t=0*, there is no oxide on the surface, which means that the thin barrier layer formed via the transformation of the airborne oxide during heat-up is neglected. The boundary conditions at the film/electrolyte interface are given by the steady-state concentrations of the respective metallic constituents at that interface obtained by the steady-state solution of the transport equations.

5.3 An approach to the outer layer growth

The outer layer is presumed to grow via the precipitation of material that is dissolved from the substrate through the inner layer of oxide. This is admittedly a simplification with regard to the real plant conditions, in which the composition of the coolant water adjacent to the outer layer plays an important role. The growth of the outer layer is a multistep process that involves the dissolution reaction at the inner layer/solution interface, already described above by the reaction steps $k_{3,i}$ (i = Fe, Cr and Ni), liquid phase transport through the pores of the outer layer, supersaturation and re-precipitation of cations both at the pore walls and at the outer layer/electrolyte interface and hence outer layer crystal growth. In the absence of representative information on the pore diameter and tortuousity, and also of reliable data on the crystallite size of the outer layer, the growth of this layer can be formally treated as a diffusion process in a matrix constituted of the outer layer crystals and the electrolyte in between. Similar treatments for a porous oxide layer have already been presented [19] and discussed in relation to incorporation of foreign species into the growing film on construction materials in nuclear power plants [20]. It has to be stressed, however, that the approach to porous layer growth outlined in the present paragraph is purely formal and it can not be considered analogous to the solid-state growth mechanism of the inner layer discussed in previous paragraphs.

Since the outer layer is not continuous, but rather represents a system of discrete crystallites with electrolyte in the pores, the role of the potential gradient in this layer can be considered negligible with respect to the concentration gradient. Thus, to calculate the depth profile of a certain cation in the outer layer, the following system of equations has to be solved:

$$\frac{\partial y_{Fe,OL}}{\partial t} = D_{Fe,OL} \frac{\partial^2 y_{Fe,OL}}{\partial x^2}$$

$$\frac{\partial y_{Cr,OL}}{\partial t} = D_{Cr,OL} \frac{\partial^2 y_{Cr,OL}}{\partial x^2} \qquad (5)$$

$$\frac{\partial y_{Ni,OL}}{\partial t} = D_{Ni,OL} \frac{\partial^2 y_{Ni,OL}}{\partial x^2}$$

The boundary conditions at the inner interface of the outer oxide layer are identical to those used as outer boundary conditions at the inner layer / electrolyte interface (see eqn. (4)), which ensures the continuity of the composition of the whole film as usually found by ex-situ analytical techniques.

It also reflects the implicit assumption that the material dissolving at the inner layer/solution boundary is effectively re-deposited to form the outer layer. In the actual in-plant case, on the contrary, we probably will not have a confined system which possibly affects the model by introducing additional terms for solution-originating Fe, Cr and Ni cations that are able to incorporate in the outer layer. This possibility is taken into account by introducing formal reaction rate constants at the boundary of the outer layer with the coolant, $k_{OL,i}$, (i=Fe,Cr, Ni etc.). These can be regarded as rate constants for release when the solubility limit of a respective cation is not reached, and rate constants for deposition if this solubility limit is exceeded. Thus the boundary conditions at the outer layer/coolant interface, $x = L_o$, where L_o is the outer layer thickness, are defined as follows

$$y_{Fe}(L_o,t) = \frac{k_{3Fe} y_{Fe}(L_i,t)}{k_{OLFe}}$$

$$y_{Ni}(L_o,t) = \frac{k_{3Ni} y_{Ni}(L_i,t)}{k_{OLNi}} \qquad (6)$$

$$y_{Cr}(L_o,t) = \frac{k_{1Cr} y_{Cr}(L_i,t)}{k_{OLCr}}$$

In the following, a steady-state is assumed, i.e. the formal reaction rate constants at the outer layer/coolant boundary are adjusted by thermodynamic values, stemming from the respective solubilities of Fe,Cr, Ni etc. [22].

5.4 Adsorption and surface complexation of solution-originating cations

The first step in the interaction between an oxide and a solution-originating cation is adsorption on the outer surface of the oxide, which is treated using the surface complexation approach. The surface hydrolysis of an oxide in hydrothermal conditions, e.g. magnetite, trevorite or hematite, can be described in terms of the 1-pK surface complexation model, in which a single surface protonation step is required [21]
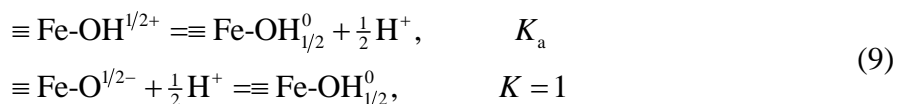
$$\equiv \text{Fe-OH}^{1/2+} = \equiv \text{Fe-O}^{1/2-} + \text{H}^+, \qquad K_a \qquad (7)$$

The mass-action equation for reaction (7) is given by

$$K_a = \frac{\left[\equiv \text{Fe-O}^{1/2-}\right]e^{-\frac{1}{2}F\psi/RT}\left[\text{H}^+\right]}{\left[\equiv \text{Fe-OH}_2^{1/2+}\right]e^{\frac{1}{2}F\psi/RT}} = \frac{\left[\equiv \text{Fe-O}^{1/2-}\right]\left[\text{H}^+\right]e^{-F\psi/RT}}{\left[\equiv \text{Fe-OH}_2^{1/2+}\right]} \qquad (8)$$

where ψ is the electrostatic potential at the interface (where the surface protons are located). The actual value of the electrostatic potential depends on the chosen surface charging model, such as Diffuse Layer Model (DLM) or the Constant Capacitance Model (CCM).

The basic species for 1-pK model is $\equiv \text{Fe-OH}_{1/2}^0$, by which both charged species in reaction (7) are written as

$$\equiv \text{Fe-OH}^{1/2+} = \equiv \text{Fe-OH}_{1/2}^0 + \tfrac{1}{2}\text{H}^+, \qquad K_a$$
$$\equiv \text{Fe-O}^{1/2-} + \tfrac{1}{2}\text{H}^+ = \equiv \text{Fe-OH}_{1/2}^0, \qquad K = 1 \qquad (9)$$

and the mass-action equations for above reactions are given by

$$K_a = \frac{\left[\equiv \text{Fe-OH}^0_{1/2}\right]\left[\text{H}^+\right]^{\frac{1}{2}}}{\left[\equiv \text{Fe-OH}^{1/2+}\right]e^{\frac{1}{2}F\psi/RT}}$$

(10)

$$1 = \frac{\left[\equiv \text{Fe-OH}^0_{1/2}\right]}{\left[\equiv \text{Fe-O}^{1/2-}\right]e^{-\frac{1}{2}F\psi/RT}\left[\text{H}^+\right]^{\frac{1}{2}}}$$

The total concentration of surface sites is calculated as the sum of neutral and charged species

$$T_{\text{Fe-OH}^{1/2}} = \left[\equiv \text{Fe-OH}^0_{1/2}\right] + \left[\equiv \text{Fe-OH}^{1/2+}\right] + \left[\equiv \text{Fe-O}^{1/2-}\right]$$

$$= \left[\equiv \text{Fe-OH}^0_{1/2}\right]\left\{1 + \frac{\left[\text{H}^+\right]^{\frac{1}{2}}e^{-\frac{1}{2}F\psi/RT}}{K_a} + \frac{1}{\left[\text{H}^+\right]^{\frac{1}{2}}e^{-\frac{1}{2}F\psi/RT}}\right\}$$

(11)

The surface charge density is accordingly

$$q_s = \frac{1}{2}\left\{\left[\equiv \text{Fe-OH}^{1/2+}_2\right] - \left[\equiv \text{Fe-O}^{1/2-}\right]\right\} = -\frac{T_{\text{Fe-OH}^{1/2}}}{2}\frac{K_a - \left[\text{H}^+\right]e^{-F\psi/RT}}{K_a\left(1 + \left[\text{H}^+\right]^{\frac{1}{2}}e^{-\frac{1}{2}F\psi/RT}\right) + \left[\text{H}^+\right]e^{-F\psi/RT}}$$
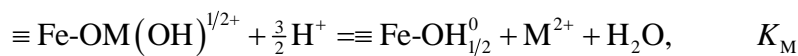
(12)

At this point, a phenomenological dependence between the surface charge and potential has to be added. Within the frames of the DLM the dependence is given by

$$\sigma_s = a_s\rho q_s = -\frac{2\varepsilon\varepsilon_0\kappa RT}{F}\sinh\left(z\frac{F\psi}{2RT}\right)$$

where

$$\kappa = 2\left(\frac{1000F^2I}{\varepsilon\varepsilon_0 RT}\right)^{\frac{1}{2}}$$

where κ is the Debye parameter (inverse thickness of the diffuse layer), a_s is the specific surface area of the sorbent, ρ is its density, ε is the dielectric constant, ε_0 is the permittivity of vacuum, and I is the stoichiometric ionic strength. Within the frames of the 1-pK surface complexation approach, the interaction of a coolant-originating cation M^{2+} with the oxide surface is written as

$$\equiv \text{Fe-OM}\left(\text{OH}\right)^{1/2+} + \tfrac{3}{2}\text{H}^+ = \equiv \text{Fe-OH}^0_{1/2} + \text{M}^{2+} + \text{H}_2\text{O}, \qquad K_M$$

5.5 Incorporation of solution-originating cations in the oxide

In order to predict quantitatively the depth profile of a solution-originating cation that is incorporated into the inner layer, we need to add the associated diffusion-migration equation for the non-steady state transport of that cation, e.g. for Zn

$$\frac{\partial c_{Zn}}{\partial t} = D_{Zn}\frac{\partial^2 c_{Zn}}{\partial x^2} - \frac{2F\vec{E}D_{Zn}}{RT}\frac{\partial c_{Zn}}{\partial x}\qquad(13)$$

to the system of equations (3) and solve the extended system subject to the boundary conditions (4). The boundary condition at the inner layer/outer layer interface is given by the enrichment factor $K_{enr,Zn,i}$ defined as the ratio between the concentration of Zn at that interface and the Zn concentration in the water: $y_{Zn}(L_i,t) = K_{enr,Zn,i}c_{Zn}(sol)$. A reflective boundary condition is used for Zn at the alloy / inner layer interface since there is usually no Zn present in the alloy substrate.

If, in addition, the solution-originating cation is present in the alloy substrate, such being the case with Co, Mn, etc., the boundary condition at the inner layer/electrolyte interface is written as

$$y_{Co}(L_i,t) = K_{enr,Co,i}c_{Co}(sol) + \frac{k_{1Co}y_{Co,a}}{V_{mo}}\left[\frac{1}{k_{3Co}} + \frac{RT}{2F\vec{E}D_{Co}}\right]$$

Within the frames of the formal model for the outer layer growth, the depth profile of e.g. Zn in the outer layer can be predicted by solving the system of equations (5) extended with a corresponding equation for Zn:

$$\frac{\partial y_{Zn,OL}}{\partial t} = D_{Zn,OL}\frac{\partial^2 y_{Zn,OL}}{\partial x^2}\qquad(14)$$

The boundary condition at the outer layer/water interface is set by the corresponding enrichment factor for the respective component at that interface, e.g. for Zn: $y_{Zn}(L_o,t) = K_{enr,Zn,o}c_{Zn}(sol)$.

5.6 Description of the calculation procedure

First, the position of the metal/film interface is determined by a sigmoidal fit of the experimental profile of the atomic concentration of oxygen obtained by the respective analytical technique - Auger Electron Spectroscopy (AES), X-ray Photoelectron Spectroscopy (XPS), Glow Discharge Optical Emission Spectroscopy (GDOES) or Secondary Ion Mass Spectroscopy (SIMS). Then, the profiles of the mass fractions of main metallic elements are normalised to the total metallic content of the film and the respective profiles are recalculated with the estimated position of the metal/film interface taken as zero. Whenever evidence of the presence of an outer layer has been found in the experimental profiles, the approximate position of the inner layer/outer layer interface is calculated by sigmoidal fits of the experimental profiles of the main metallic constituents of the alloy – Fe and Cr for stainless steels, or Ni and Cr for nickel-based alloys.

As a first step of the calculation, the system of equations (3) is solved subject to the initial and boundary conditions (4) using a Crank-Nicholson method in order to obtain the compositional profiles in the inner layer. In the cases when an outer layer is present, the inner layer thickness has been subtracted and the inner/outer layer boundary is taken as a new zero. Then the system of equations (5) is solved with the respective boundary conditions at the inner layer/outer layer interface similar as those used in (4). The boundary conditions at the outer layer / electrolyte interface are at this point assumed to be equal to the experimentally found

stoichiometry of the outermost layer of oxide as determined by the respective ex-situ technique. The surface composition has been found to be in reasonable agreement with thermodynamic calculations of the solubility of the respective oxide phases discussed by other authors [22]. As a final step, the calculated profiles for the normalised mass fractions of the inner and outer layers are combined in order to compare the model predictions with the experimental results in a convenient way. It has to be stressed that the outlined procedure does not represent an optimisation method per se, but rather a manual search for the best possible match between the experimental and calculated profiles by a trial-and-error method. In that respect, the possibility of another set of parameters furnishing an equally good fit to the experimental data can not be excluded. Proofs of the reliability of the estimated kinetic and transport parameters are sought a posteriori by computing further characteristics of the systems under study. The adopted procedure of validation of the model is described below, using results from ex-situ characterisation of oxides formed on stainless steels and nickel-based alloys in both real (in-reactor) and simulated BWR, PWR and WWER coolant cases.

6 Results and Discussion

6.1 Pressurised Water Reactor case

6.1.1 Effect of exposure time and Zn addition on the kinetic parameters of film growth on AISI 304 stainless steel

The experimental and calculated depth profiles of the mass fractions of Fe, Cr and Ni in the oxides formed on AISI 304 stainless steel in simulated PWR water without Zn addition at 260ºC for 5000 and 10 000 h are shown in Fig. 5. The corresponding profiles obtained in simulated PWR water with the addition of 30 ppb of Zn after 1000 and 10 000 h of oxidation are presented in Fig. 6. Double-layer oxides are formed in both environments, the inner layers being slightly enriched in Cr whereas the outer layers contain mostly Fe and Ni. The oxides formed in the presence of Zn are significantly thinner than those in the absence of Zn, and significant amounts of Zn are incorporated in the outer part of the inner layer. The profile of Zn in the inner layer follows to a certain extent that of Cr, and the enrichment of Cr in the Zn-doped inner layers is more significant than that in the inner layers formed in the absence of Zn. The outer layer is significantly thinner than the inner layer in the presence of Zn, especially for a 10 000 h of exposure.

The calculated profiles (shown in the figures with solid lines) match sufficiently well the experimental ones, except for the profile of Zn in the vicinity of the alloy/inner layer interface. This could be due to sputtering effects since no Zn is expected to be present in the base alloy. The values of the kinetic parameters calculated from the simulation are shown in **Fig. 7** (rate constants at the alloy/inner layer and inner layer/electrolyte interfaces) and **Fig. 8** (diffusion coefficients in the inner layer and formal diffusion coefficients of the growth of the outer layer, respectively).

The profiles obtained after 5000 and 10000 h of exposure in an electrolyte without Zn are reproduced with a rather homogeneous set of parameters, this being especially true for the rate constants at both interfaces. The rate constant for oxidation of Cr at the inner interface is the highest whereas the corresponding rate constant for dissolution of Cr at the outer interface is the lowest, which results in the observed Cr enrichment in the outer part of the inner layer. The opposite is true for Fe which is preferentially leached from the inner layer and subsequently redeposited to form the outer layer, as observed in the profiles.
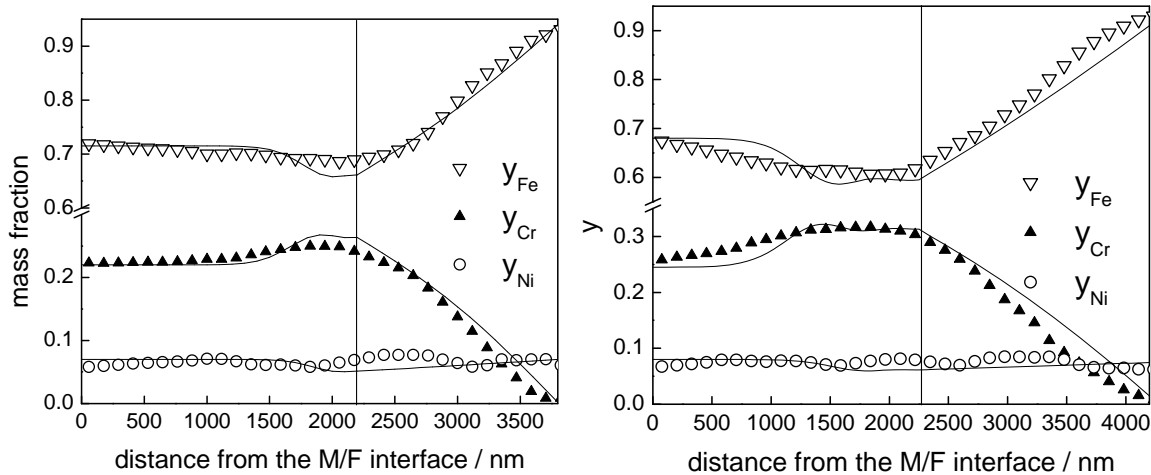
Fig. 5 Experimental (points) and calculated (solid lines) XPS depth profiles of the mass fractions of Fe,Cr, and Ni in the films formed on AISI 304 during a 5000 h (left) and 10 000 h (right) exposure to a simulated PWR water at 260 °C. The inner layer / outer layer boundary indicated with a vertical line. Experimental data from Ref. 23.
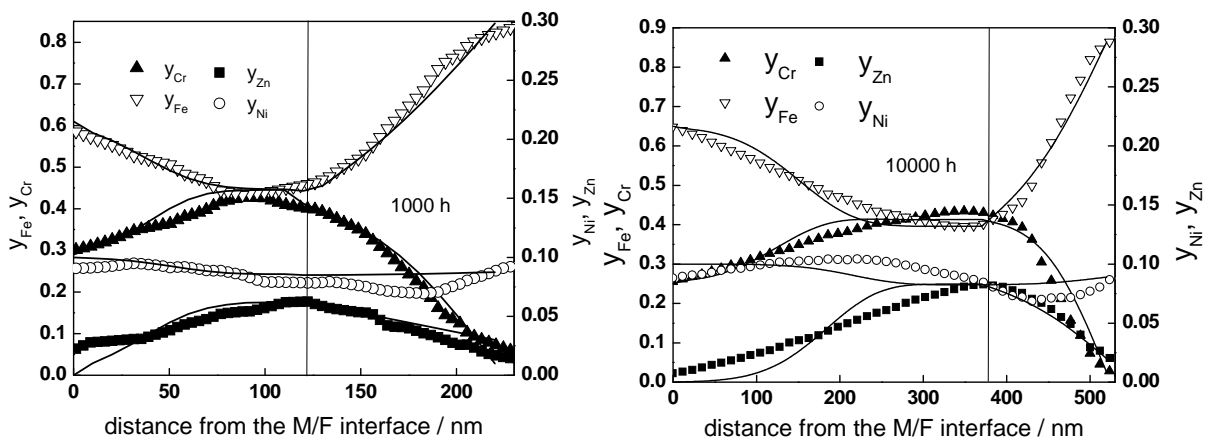

Fig. 6 Experimental (points) and calculated (solid lines) XPS depth profiles of the mass fractions of Fe,Cr, Ni and Zn in the films formed on AISI 304 during a 1000 and 10,000 h exposure to a simulated PWR water with the addition of 30 ppb Zn at 260 °C. The inner layer / outer layer boundary indicated with a vertical line. Experimental data from Ref.24.

The effect of Zn on the kinetic and transport parameters is significant, especially on the diffusion coefficients in the inner layer and the formal diffusion coefficients depicting the growth of the outer layer of oxide. In other words, when the film grows in an electrolyte containing Zn, the transport rate in the inner layer of oxide has been reduced by a factor of 3-4, and the growth of the outer oxide is almost totally suppressed, especially for longer oxidation times (**Fig. 8**).

The decreasing effect of Zn on the kinetics of the interfacial reactions is comparatively weaker, with one notable exception – in solutions containing Zn, the rate constant of Fe dissolution from the inner layer is somewhat larger than that in electrolytes without Zn addition (**Fig. 7**). It is tempting to assume that Zn is substituted for divalent Fe, thus expulsing the latter from the oxide, as already discussed by several authors [24-26].

The following line of reasoning is proposed to explain these observations. If the incorporation of Zn at the inner layer/electrolyte interface occurs via filling of available empty cation interstices V_i and/or cation vacancies V_M'' :

$$V_i + Zn_{aq}^{2+} \rightarrow Zn_i^{\bullet\bullet} \tag{15}$$

$$V_M'' + Zn_{aq}^{2+} \rightarrow Zn_M' \tag{16}$$

then the concentration of these defects at the interface will decrease. In order their steady-state concentration to be maintained, an additional amount of Fe (the main element of the alloy) has to dissolve according to the reactions

$$Fe_i^{\bullet\bullet} \rightarrow Fe_{aq}^{x+} + V_i + (x-2)e' \tag{17}$$

$$Fe_{Fe}^{X} \rightarrow Fe_{aq}^{x+} + V_M'' + (x-X)e' \tag{18}$$

According to the model described above, the sum of the rate constants of the reactions (17) and (18) is equal to the rate constant k_{3Fe}, which is observed to increase with the addition of Zn to the electrolyte. Further incorporation of Zn in the bulk of the inner layer will lead to a decrease of the concentration of defects, and also their mobilities, within the oxide. This in turn explains the much smaller values of the diffusion coefficients of inner layer constituents when the film is grown in solutions that contain Zn.

The sum of the reactions (15)-(18) can be written as an equilibrium exchange between a Fe cation in the inner layer of oxide and a Zn aquoion in the electrolyte, in analogy with what has been proposed in Ref. 24:

$$Fe_{inner\ layer} + Zn_{aq}^{2+} \rightleftarrows Fe_{aq}^{x+} + Zn_{inner\ layer} \tag{19}$$

Alternatively, the first step of Zn incorporation in the oxide can be written as a surface complexation reaction [21]

$$\equiv Fe-OH_{1/2}^{0} + Zn_{aq}^{2+} \rightleftarrows \equiv Fe-OZn^{1/2+} + H^{+} \tag{20}$$
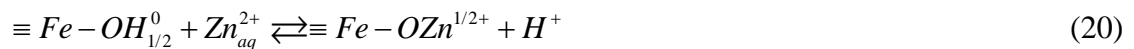
The equilibrium constant of this reaction on magnetite has been estimated to be 41.7 at 280°C using the constant capacitance model to quantitatively interpret high-temperature titration data on magnetite surfaces in simulated PWR water [27]. The equilibrium constant can be also estimated from the present results using data on the mass fractions of Zn and Fe at the inner layer/electrolyte interface (Fig. 6), the surface site concentration on magnetite estimated earlier from titration data (1.75×10^{-10} mol cm^{-2}) and the speciation of soluble Zn in the electrolyte calculated using literature data [27]. A value of 60 ± 10 is obtained, in reasonable agreement with the surface complexation calculations. It can be concluded that the first step of Zn incorporation into the oxide is described adequately by the surface complexation model and equation (20). It is worth noting that recent estimates of the surface site concentration and the point of zero charge of trevorite in hydrothermal conditions [28] demonstrate that the above interpretation remains valid also for the interaction of Zn with trevorite.
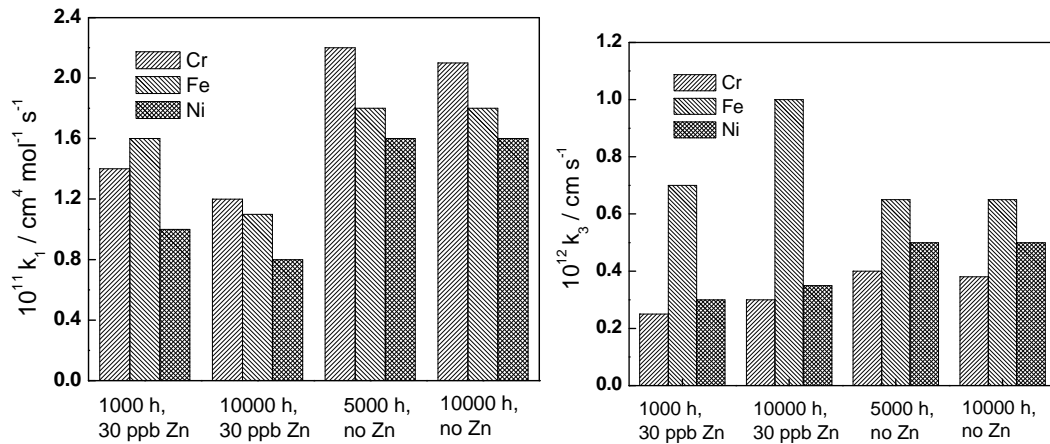
Fig. 7 Dependence of the rate constants for inner layer constituents at the alloy/inner layer (left) and inner layer/electrolyte (right) interfaces on time of exposure and Zn addition.
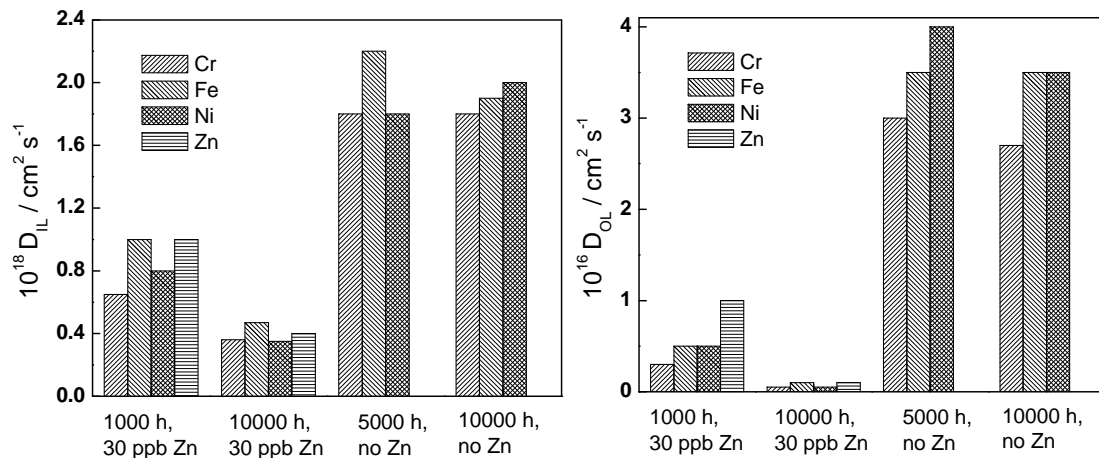

Fig. 8 Dependence of the diffusion coefficients of inner layer constituents (left) and formal diffusion coefficients depicting the growth of the outer layer (right) on time of exposure and Zn addition.

6.1.2 Effect of Zn on in-reactor Co incorporation in the oxide on stainless steel

The effect of Zn on the incorporation of radioactive matter (e.g. Co) from the coolant into the oxides formed on stainless steels and nickel-based alloys has been thoroughly investigated by the Halden Reactor project [29-31]. Both fresh and preoxidised samples have been exposed to PWR in-plant conditions (1000 ppm B, 3 ppm Li, 320 ºC, $pH_{300ºC} = 7.1$, soluble Zn either 0 or ca. 50 ppb, soluble Co ca. 0.05 ppb), the duration of each exposure phase being ca. 100 Effective Full Power Days (EFPD). The SIMS depth profiles for Fe, Cr, Ni, Co, Mn and Zn in the films obtained after the first and third exposure phase on fresh AISI 304 sample in the presence of 50 ppb Zn in the water are shown in **Fig. 9** together with the profiles calculated using the present model. The kinetic and transport parameters estimated from the calculation are collected in **Fig. 10**. The following conclusions can be drawn on the basis of the parameter values:

- The set of parameters used to simulate the in-reactor film growth and restructuring on AISI 304 is fully compatible with that used for the simulation of the growth and restructuring on the same steel in laboratory conditions (see previous paragraph). This

demonstrates the feasibility of the present model also for the interpretation of in-reactor data.

- The equilibrium constant of Co incorporation via a reaction analogous to (20) was estimated to be close to 1, which agrees by order of magnitude with the value calculated on the basis of high-temperature titration data and the surface complexation model [27], whereas the corresponding value for Zn incorporation was again of the order of 50, confirming the earlier calculations and demonstrating once again the higher affinity of Zn towards the surface oxide.

- The main effects of Zn are on the values of the diffusion coefficients in both layers and to a certain extent on the values of the rate constants at the outer interface. This can be interpreted as a modification of both the oxide surface and the bulk oxide by Zn addition.

- Oxide growth/restructuring and incorporation of Co in the oxide are retarded by Zn incorporation. This could be related to the formation of new Zn-containing phases in both the inner and outer layers, as discussed also by other authors [24-26,31].

The SIMS depth profiles for Fe, Cr, Ni, Co and Zn in the films obtained after in-reactor exposure of a preoxidised AISI 304 sample to PWR water in the presence or absence of Zn are shown in **Fig. 11** together with the corresponding profiles calculated by the model. The kinetic and transport parameters estimated from the calculation are collected in **Fig. 12**. On comparing the parameter values for the fresh and preoxidised samples, it can be concluded that:

- Incorporation of Zn in already existing oxides is slower, and the layer restructuring is less pronounced. The diffusion coefficients in the inner layer formed in the presence of Zn on the preoxidised samples are ca. 50% lower than those formed on the fresh sample, and when the Zn-doped oxide is once again exposed to Zn-free PWR water, their initial values are restored. This means that the incorporation of Zn in pre-existing oxides is to a great extent reversible, thus less effective in suppressing further oxide growth and incorporation of solution-originating Co.

- There is no appreciable difference between the values of the apparent diffusion coefficients in the outer layer in both cases, with the notable exception of the diffusion coefficient for Co - when Zn is added, $D_{Co,OL}$ decreases to a half of its value before Zn addition. Thus Zn addition suppresses incorporation of Co in the outer layer as well.

- The value of the rate constant k_{3Fe} is once again much higher in the presence of Zn which could be interpreted as if the exchange reaction of Zn for Fe being efficient enough for preoxidised samples as well and its mechanism being essentially unaltered.
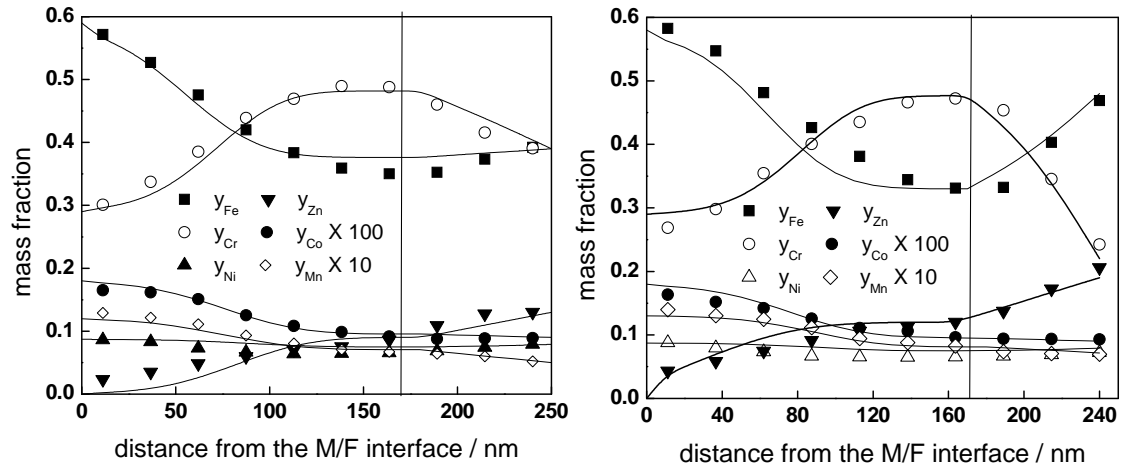
Fig. 9 *Experimental (points) and calculated (solid lines) depth profiles of the mass fractions of Fe, Cr, Ni, Co, Mn and Zn in the films formed on AISI 304 after the exposure to ca. 100 and 300 EFPD (125 and 336 days) in the Halden Reactor, PWR coolant conditions. The inner layer / outer layer boundary indicated with a vertical line. Experimental data taken from Refs 29-31.*
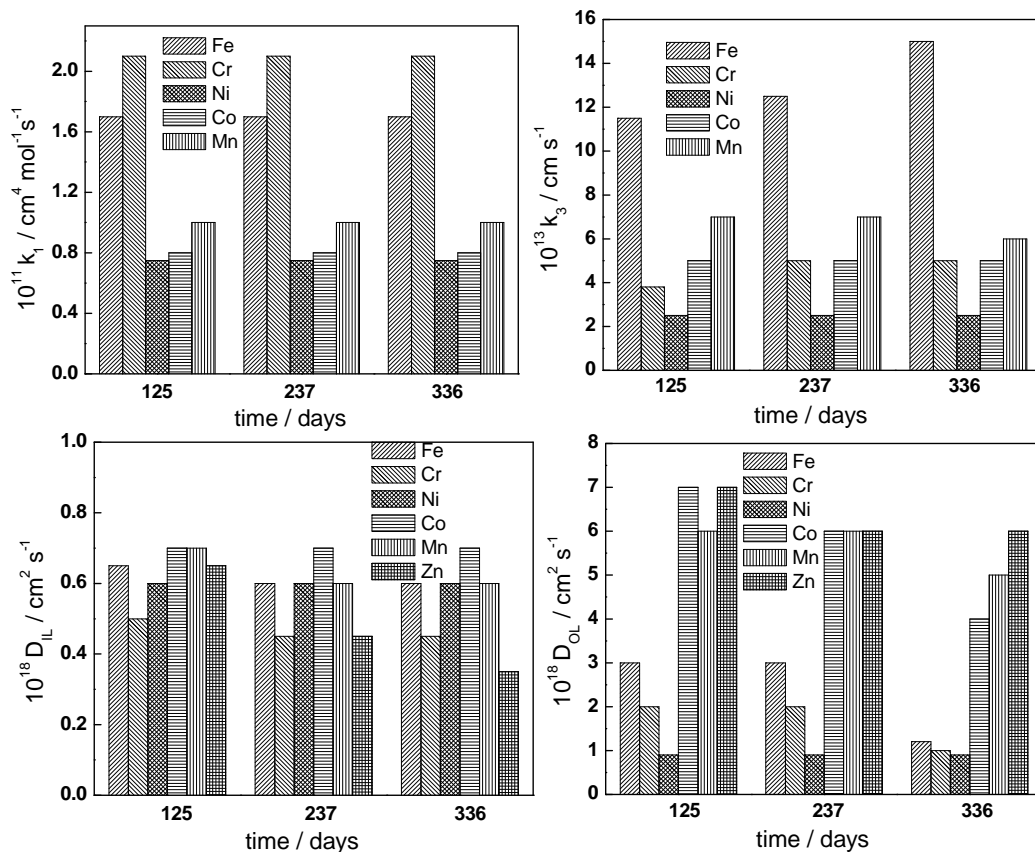

Fig. 10 *Dependence of the rate constants at the steel/inner layer interface (above left), the inner layer/electrolyte interface (above right), diffusion coefficients of inner layer constituents (below left) and formal diffusion coefficients depicting the growth of the outer layer (below right) on time of exposure. 50 ppb Zn added from the beginning of exposure.*

A summary plot of the estimated values of the field strength in the inner layer of the oxide on AISI 304 is given in **Fig. 13**. The values of the field strength in the inner layers formed or restuctured in the presence of Zn in the water are somewhat higher than those in the absence of Zn, and a slight decrease of this parameter with time of exposure is observed. Overall, the

effect of both time of exposure and Zn addition to the electrolyte is small and the field strength can be considered essentially constant, its values being in agreement with what has been calculated earlier by us in the same temperature range [17]. The values of the field strength are in general rather low and confirm the validity of the low-field approximation used to derive the model equations in the Theory section.
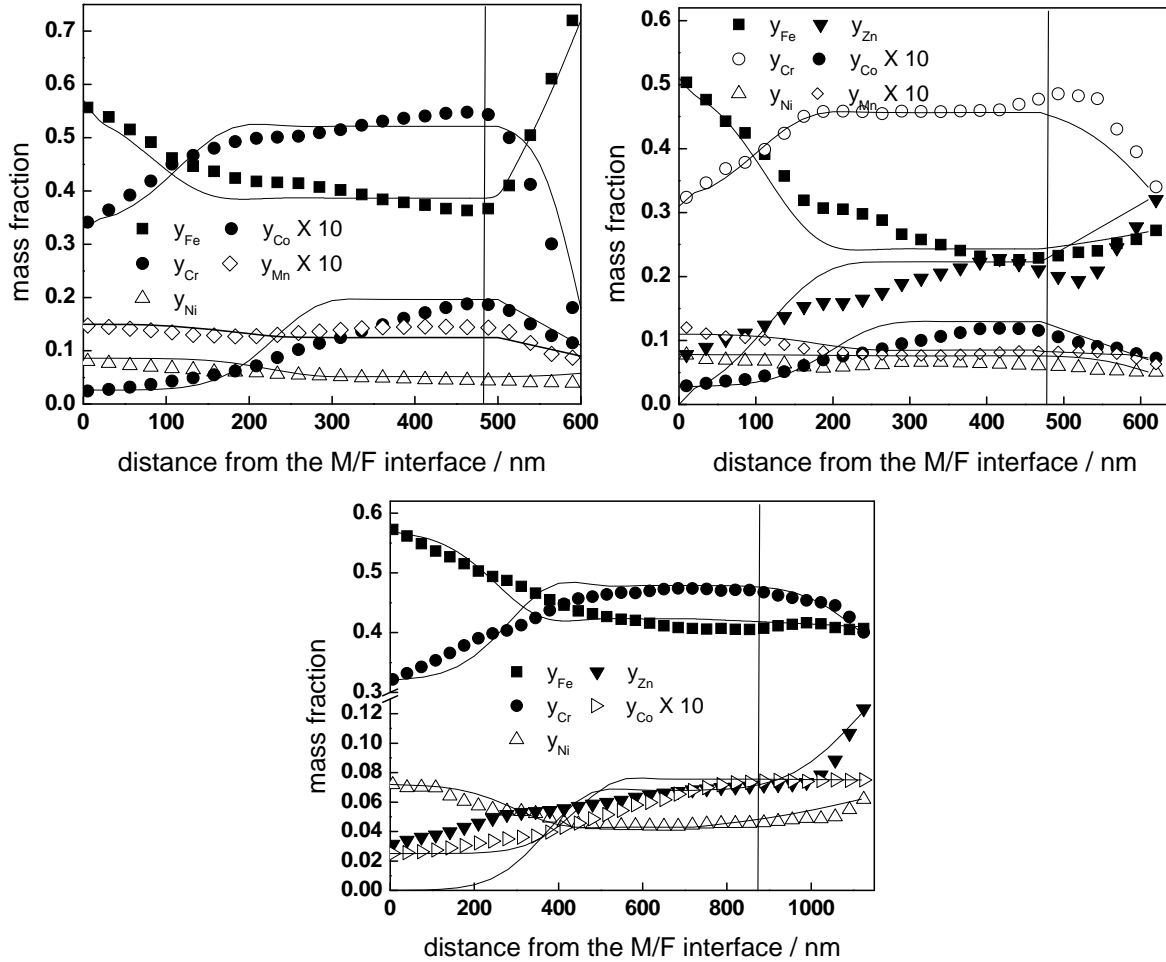

Fig. 11 *Experimental (points) and calculated (solid lines) depth profiles of the mass fractions of Fe, Cr, Ni, Co, Mn and Zn in the films formed on AISI 304 during a 100 day exposure with no Zn addition (above left), followed by a 237 day exposure to 50 ppb Zn (above right) and another 230 day exposure with no Zn addition (below). The inner layer / outer layer boundary indicated with a vertical line. Experimental data taken from Refs 29-31. Data for Mn for the second exposure to Zn-free coolant not available.*

Further proof for the validity of the model comes from Fig. 14, in which the inner layer thicknesses for the oxides formed on AISI 304 in both simulated and in-reactor PWR water in the absence or presence of Zn are compiled as depending on exposure time (data from Refs. 23-34). In the figure, experimentally determined thickness values are compared with the thickness calculated according to the relationship proposed within the frames of the PDM and MCM [3,17]

$$L(t) = L(t = 0) + \frac{1}{b} \ln \left[1 + V_{m,MO} (k_{1,Cr} y_{Cr,a} + k_{1,Fe} y_{Fe,a} + k_{1,Ni} y_{Ni,a}) b e^{-bL(t=0)} t \right]$$

(21)

$$b = \frac{3\alpha_1 F \vec{E}}{RT}$$

subject to the assumption that the transfer coefficients for all the three reactions at the metal film interface are similar and equal to α_1 and the values of the rate constants are taken from **Fig. 7**, **Fig. 10** and **Fig. 12**. Notwithstanding the fact that the compilation of data is stemming from exposure to slightly different experimental conditions, the solid lines shown in **Fig. 14** demonstrate the fair agreement between the experimentally estimated thicknesses and model predictions, which is encouraging taking into account the fact that no further adjustment has been made.
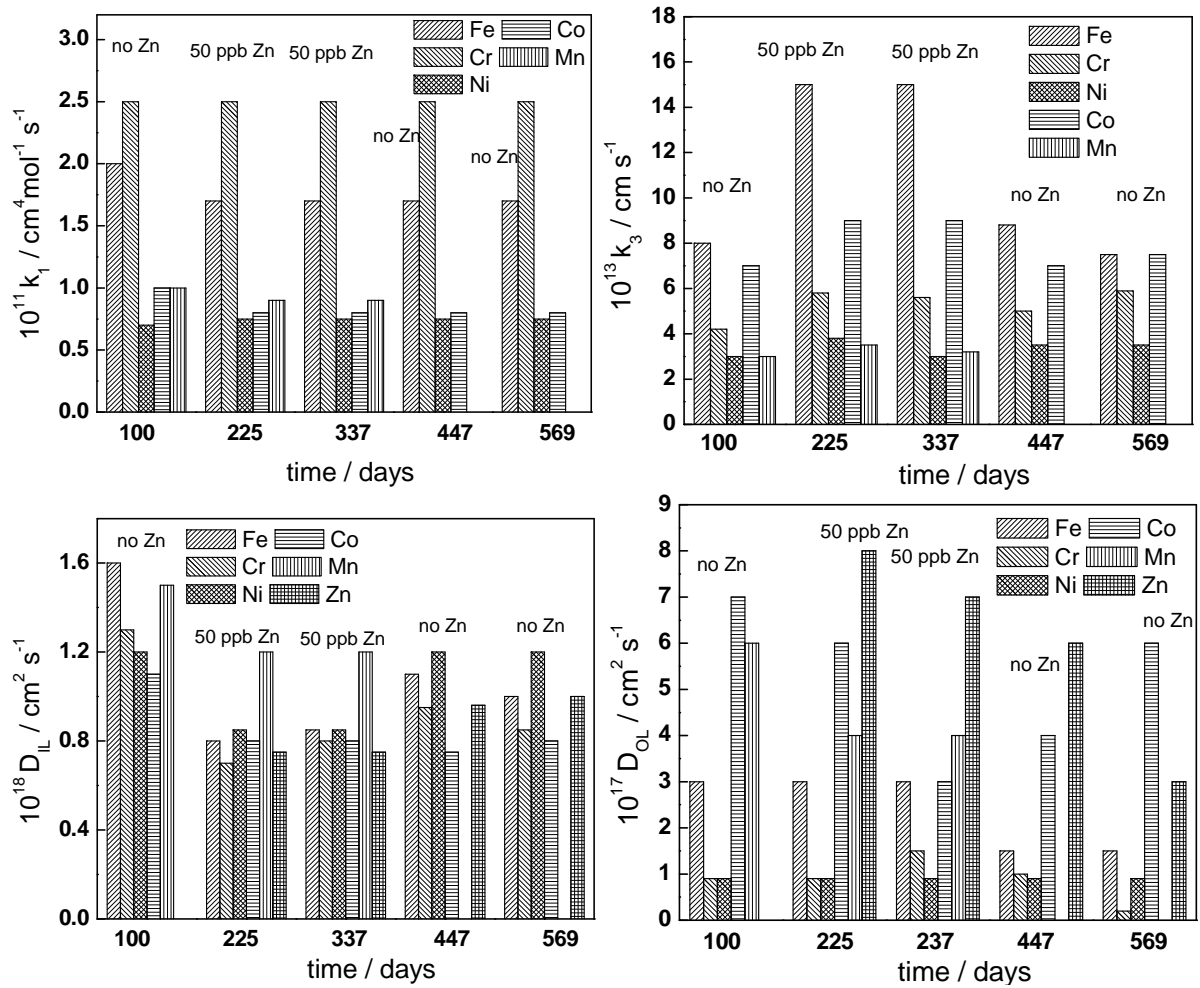
Fig. 12 Dependence of the rate constants at the steel/inner layer interface (above left), the inner layer/electrolyte interface (above right), diffusion coefficients of inner layer constituents (below left) and formal diffusion coefficients depicting the growth of the outer layer (below right) on time of exposure of AISI 304 to PWR water. Successive periods without and with Zn as indicated.
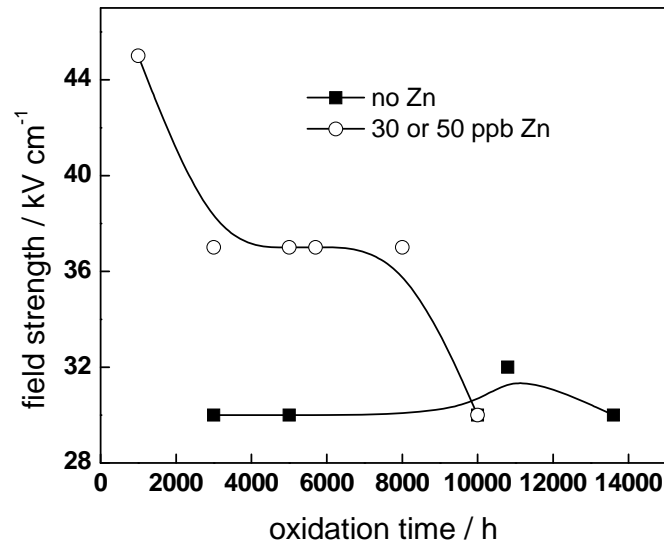
Fig. 13 Summary of the field strength values for the inner layer on AISI 304 calculated from the comparison of the model equations to the data in Fig. 5,Fig. 6,Fig. 9 and Fig. 11.
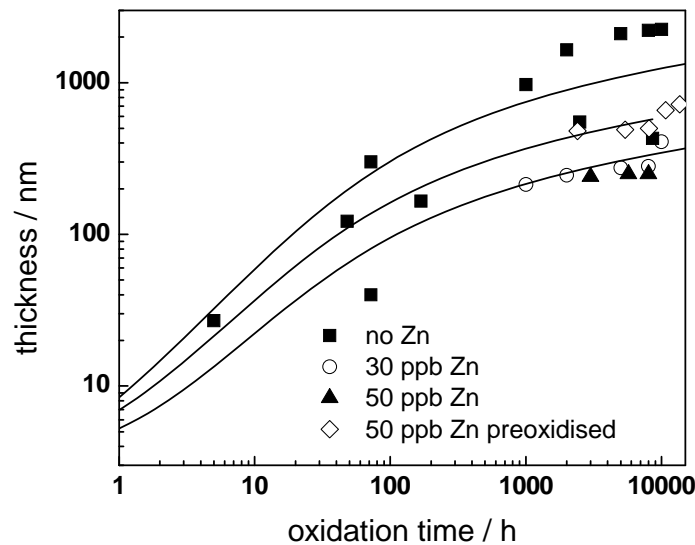

Fig. 14 Inner layer thickness vs. time data for AISI 304 in simulated and in-reactor PWR water with or without Zn addition at 260-300 °C (symbols) and calculated curves according to the model (solid lines).

6.1.3 Effect of exposure time and Zn addition on the kinetic parameters of film growth on nickel-based alloys

Knowledge of the oxidation processes on Ni alloys in a PWR coolant is of major importance for at least two practical reasons: (i) the radioactivity of the primary circuit is primarily due to cations released by corrosion of the steam generator tubes made mainly of nickel-based alloys and (ii) the oxidation process is important in the mechanisms of the initiation of intergranular stress corrosion cracking in Alloys 600, 82 and 182. Understanding the root causes of this cracking should also allow the safety margins offered by the Alloys 690, 52 and 152, which have replaced the former ones, to be evaluated more accurately. Very recently, unique experiments and new data on the initial stages of passive oxide film growth on nickel-based Alloys 600, 690 and 800 in a simulated PWR coolant using a micro-autoclave technique

combined with *ex situ* XPS and STM characterisations have been reported [35-37]. A preliminary treatment of these data in terms of the MCM using a set of parameters calculated from fitting of electrochemical impedance spectroscopic data on binary Ni-15%Cr and Ni-20%Cr alloys has been presented and discussed in Ref. 16. Further treatment of these and associated data to extract the full set of model parameters as depending on exposure time and also Zn addition to both simulated and in-reactor PWR water is given in the present chapter.

Fig. 15 shows XPS depth profiles of the mass fractions of Ni, Cr and Fe in the oxides formed on Alloy 600 in simulated PWR water (2 ppm Li, 1200 ppm B, partial pressure of H_2 0.3×10^5 Pa) for 20 and 100 h at 325ºC [35] together with the corresponding profiles calculated by the model. XPS depth profiles for the oxides on Alloy 600 stemming from experiments involving much longer oxidation times in simulated PWR water with and without the addition of 30 ppb of soluble Zn at 260ºC [38,39] are presented in **Fig. 16** and **Fig. 17**, respectively. The parameters used to reproduce the experimental profiles are collected in **Fig. 18**. On the other hand, XPS depth profiles of the mass fractions of Ni, Cr and Fe in the oxides formed on Alloy 690 in simulated PWR water for 20, 50 and 100 h at 325ºC are summarized in **Fig. 19**, and the corresponding parameters used to calculate the profiles are collected in **Fig. 20**-**Fig. 21**.
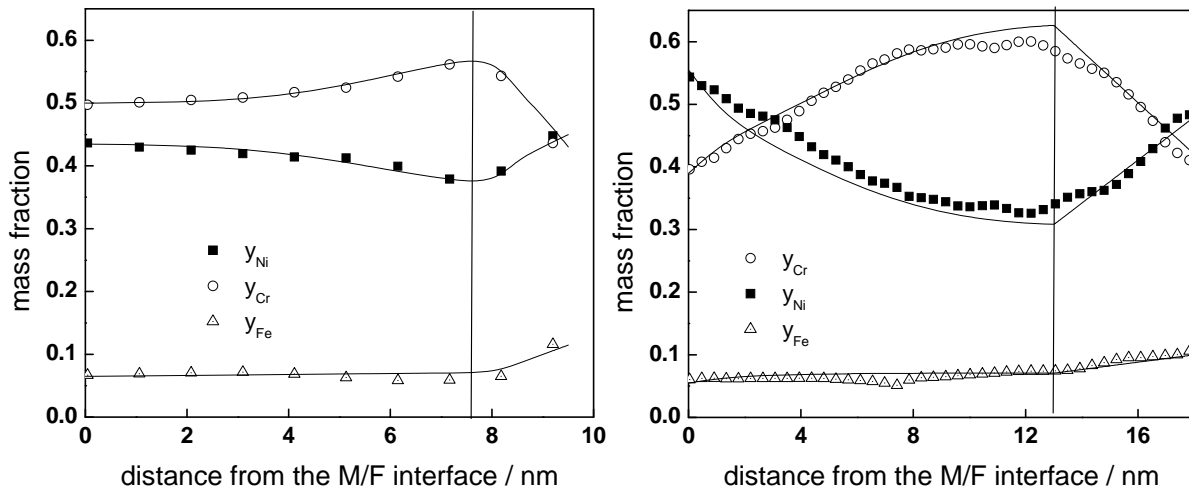

Fig. 15 Experimental (points) and calculated (solid lines) depth profiles of the mass fractions of Fe, Cr, and Ni in the films formed on Alloy 600 in simulated PWR water for 20 h (left) and 100 h (right). The inner layer / outer layer boundary indicated with a vertical line. Experimental data taken from Ref. 35.

Concerning in-reactor exposure, SIMS depth profiles for Fe, Cr, Ni, Co and Zn in the films obtained on a fresh Alloy 690 sample after the first and third exposure phase of the Halden reactor project experiment discussed above in the presence of 50 ppb Zn in the water are shown in **Fig. 22** together with the profiles calculated using the present model. The kinetic and transport parameters estimated from the calculation are collected in **Fig. 23** and **Fig. 24**.
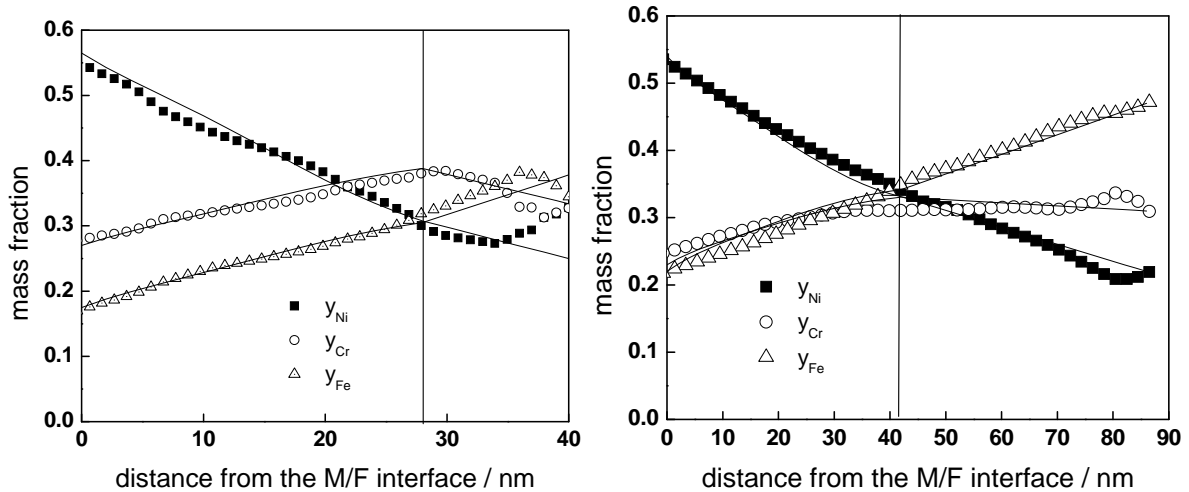
Fig. 16 *Experimental (points) and calculated (solid lines) depth profiles of the mass fractions of Fe, Cr, and Ni in the films formed on Alloy 600 in simulated PWR water for 5000 h (left) and 10000 h (right). The inner layer / outer layer boundary indicated with a vertical line. Experimental data taken from Ref. 38.*
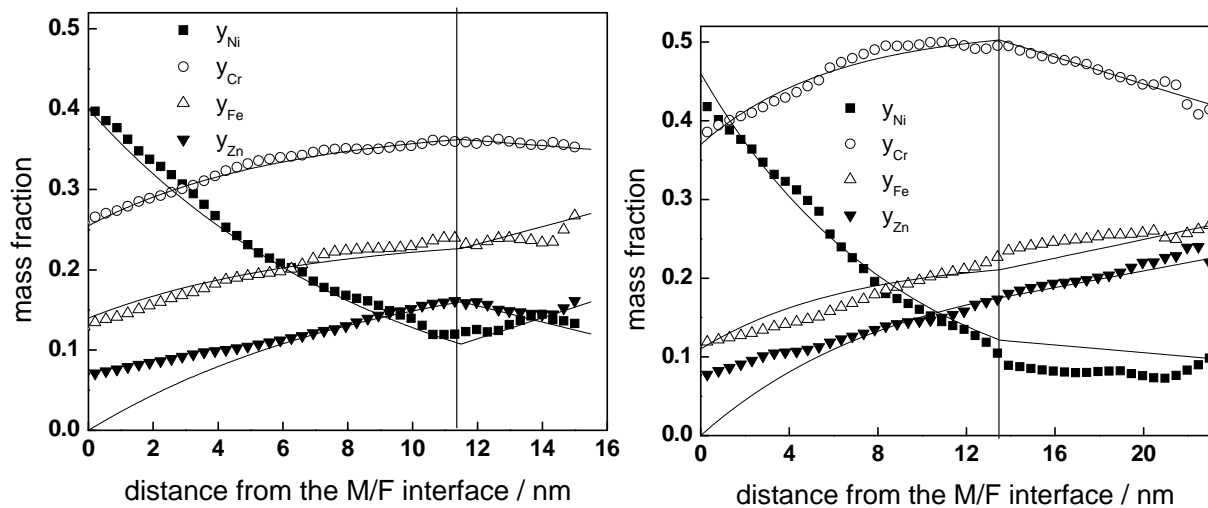

Fig. 17 *Experimental (points) and calculated (solid lines) depth profiles of the mass fractions of Fe,Cr, Ni, and Zn in the films formed on Alloy 600 in simulated PWR water with 30 ppb Zn for 5000 h (left) and 10000 h (right). The inner layer / outer layer boundary indicated with a vertical line. Experimental data taken from Ref. 39.*

Several differences can be noticed between the estimated parameter values for the oxides on stainless steels and nickel-based alloys when comparing **Fig. 7**, **Fig. 8**, **Fig. 10**,**Fig. 12**, **Fig. 18**, **Fig. 20**, **Fig. 21**, **Fig. 23** and **Fig. 24**:

- The differences between parameters for oxides on Alloys 600 and 690 is not very significant, the only important difference being observed for the diffusion coefficients in the inner layer (**Fig. 21**, left). In general it can be stated that the values of the parameters on Alloy 690 are somewhat larger and their time evolution more pronounced. The lower diffusion coefficients in the inner layer on Alloy 600 can be tentatively explained by the unavailability of Cr from the alloy layer underneath the oxide, which retards film growth, as suggested in Refs. 35-37.

- The diffusion coefficients of individual constituents of the inner layer are significantly (more than an order of magnitude) smaller for the oxides formed on nickel-based alloys, which explains the much slower growth and restructuring of the corrosion layers on these materials when compared to stainless steels. This fact can be in general explained by the composition of the inner layer, which is close to chromium oxide (Cr_2O_3) for nickel-based alloys, whereas it can be considered as close to the normal spinel chromite ($FeCr_2O_4$) on stainless steels. The diffusion coefficients in spinel structures are in general much larger than those in corundum structures as that of Cr_2O_3.

- There is also a very significant difference between the formal diffusion coefficients of the outer layers formed on stainless steels and nickel-based alloys which amounts to more than two orders of magnitude in certain cases. A tentative explanation for this observation could be that the growth mechanism of the outer layer on nickel-based alloys (which consists of NiO or $Ni(OH)_2$, or a mixture of the two and $NiFe_2O_4$) is closer to a solid-state process, whereas the outer layer on stainless steels (consisting mainly of trevorite $NiFe_2O_4$ doped with Cr) grows via a dissolution-precipitation reaction resulting in comparatively large crystals with electrolyte in between.
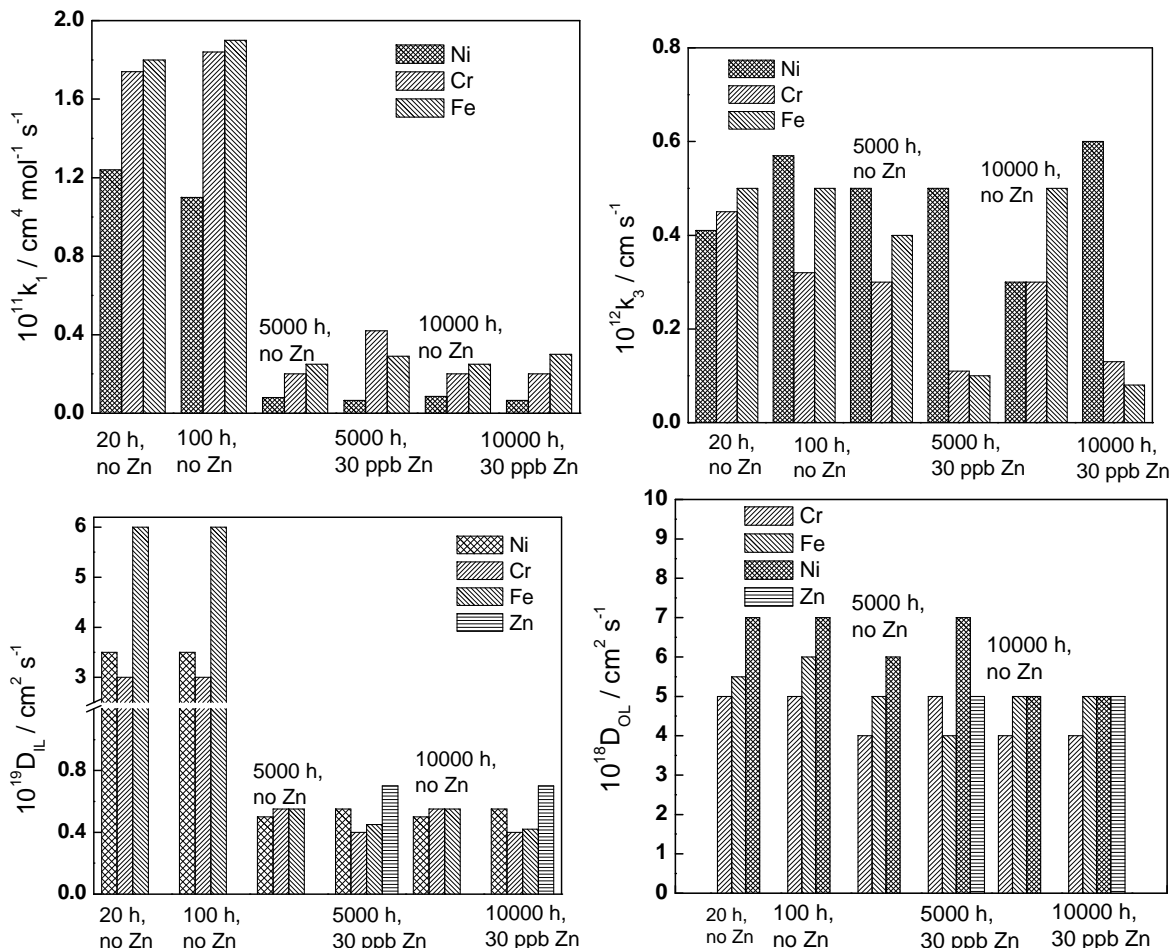

Fig. 18 Dependence of the rate constants at the alloy 600 / inner layer interface (above, left), inner layer/electrolyte interface (above,right), diffusion coefficients of inner layer constituents (below left) and formal diffusion coefficients for the growth of the outer layer (below right) on time of exposure to simulated PWR water with or without Zn addition.

- On the other hand, the differences between the interfacial rate constants at the inner and outer interfaces are much smaller, although there is some tendency for a decrease

of the rate constants at the inner layer /electrolyte interface from the oxide on stainless steels to that on nickel-based alloys. Thus the mechanism of the interfacial reactions does not seem to be altered remarkably by the transition of the main element in the alloy from Fe to Ni.

Concerning the effect of Zn on the oxide growth and restructuring, it can be stated that the effect is much smaller on the oxides formed on Ni-based alloys than on those formed on stainless steels, even if the amounts of incorporated Zn especially in the outer part of the inner layers on both types of materials are not very different. It can be argued that the incorporation of Zn in a Cr_2O_3 type structure does not lead to such a large alteration of the properties of such phase when compared to the incorporation of Zn in $FeCr_2O_4$ type oxides.

Indeed, by examining the values of the diffusion coefficients of inner layer constituents of the oxide on nickel-based alloys, it can be concluded that the time of exposure has a much larger influence on the values than the addition of Zn to the electrolyte. In order to explain the effect of film aging on its properties, the effect of microstructure has to be considered.
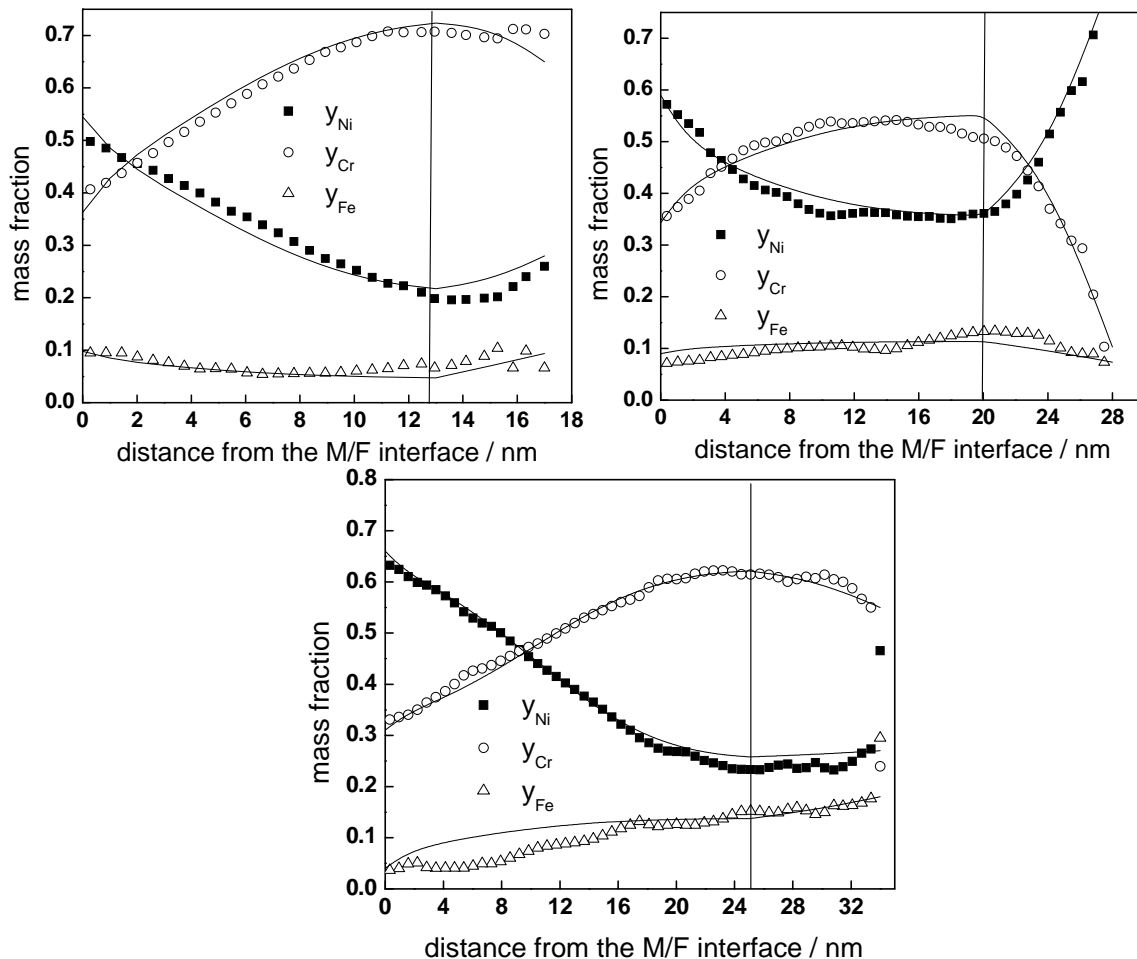

Fig. 19 Experimental (points) and calculated (solid lines) depth profiles of the mass fractions of Fe,Cr, and Ni in the films formed on Alloy 690 in simulated PWR water at 325 for 20 h (above, left), 50 h (above, right) and 100 h (below). The inner layer / outer layer boundary indicated with a vertical line. Experimental data taken from Ref. 35.
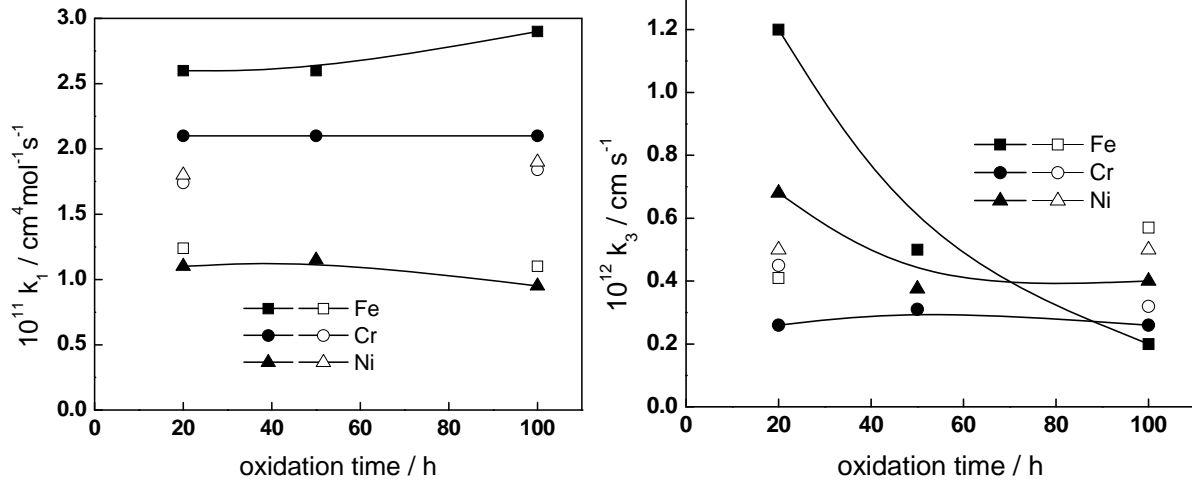
Fig. 20 *Dependence of the rate constants at the alloy 690 / inner layer interface (left) and the inner layer/electrolyte interface (right) on the time of exposure of Alloy 690 to simulated PWR water (full symbols). The values for the oxide on Alloy 600 are shown with open symbols for comparison.*
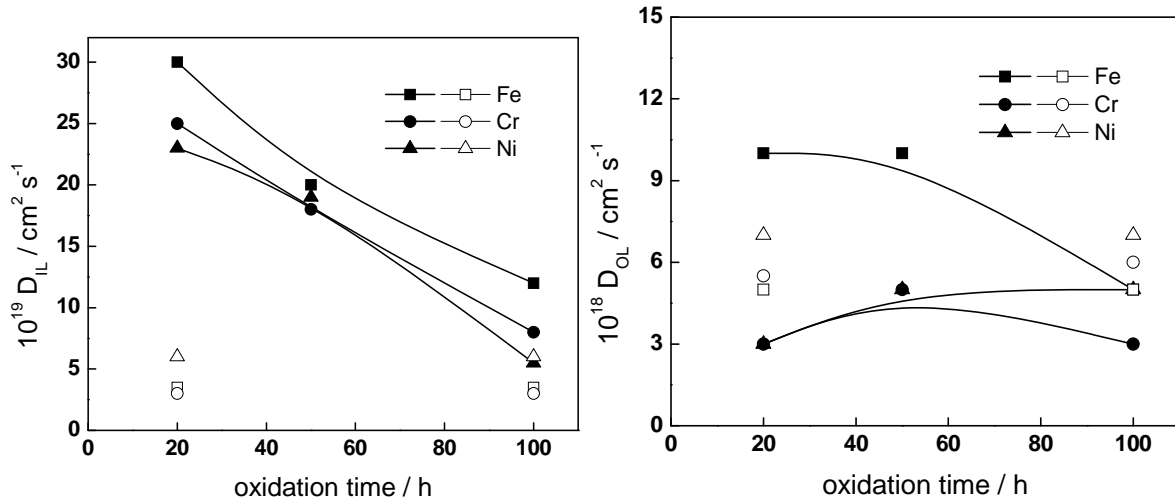

Fig. 21 *Dependence of the diffusion coefficients of inner layer constituents (left) and formal diffusion coefficients for the growth of the outer layer (right) on the time of exposure of Alloy 690 to simulated PWR water (full symbols). The values for the oxide on Alloy 600 are shown with open symbols for comparison.*

In the simplest treatment, the effective diffusion coefficient can be expressed as a combination of the diffusion coefficients in the grain interior and at the grain boundary

$$D_{eff} = (1 - f_{gb})D_{gi} + f_{gb}D_{gb} \tag{22}$$

where for the fraction of grain boundaries the following equation holds as a first approximation

$$f_{gb} \approx \frac{3\delta_{gb}}{\Phi} \tag{23}$$

where δ_{gb} is the grain boundary width (of the order of 1 nm) and Φ is the grain size of the oxide in question. An additional explanation for enhanced conduction at boundaries is related to the formation of space charge regions in the grain areas adjacent to the boundaries. As charged species and defects tend to segregate to the grain boundaries to lower the strain and electrostatic energy of the system, the boundary charges are compensated by the formation of space charge in the adjoining grain areas. If a bulk defect with a high mobility is accumulated in the space charge region, the overall conductivity of the solid should increase. The width of the space charge region can be linked to the space charge screening length

$$L_D = \sqrt{\frac{\varepsilon\varepsilon_0 kT}{e^2 N}} \tag{24}$$

Using typical values for $\varepsilon=20$, $T=573$ K and a bulk concentration of the high mobility carrier $N = 5 \times 10^{19}$ cm^{-3}, we arrive at $L_D = 5$ nm, which can be substituted for δ_{gb} in equation (23).

Using data from Refs. 35-39, an increase of grain size of the oxide on Alloy 600 from 10 to 30 nm is adopted for oxidation between 20 and 5000 h, and a corresponding decrease of the fraction of grain boundaries from 0.3 (at 20 h) to 0.1 (at 5000 h) is obtained from equations (23)-(24). Using the calculated value of the diffusion coefficient e.g. for Ni after 20 and 5000 h of oxidation (**Fig. 18**), the grain interior diffusion coefficient is estimated as 10^{-20} cm^2 s^{-1} in good agreement with an extrapolation of the diffusion coefficient of Ni for dry oxidation in the intermediate temperature range [40]. Although this can be considered as a proof for the validity of the present approach to the heterogeneity of the inner layer of oxide as a transport medium, the availability of grain size data for the inner corrosion layers in high-temperature water is not sufficient to generalize this treatment for other structural materials.
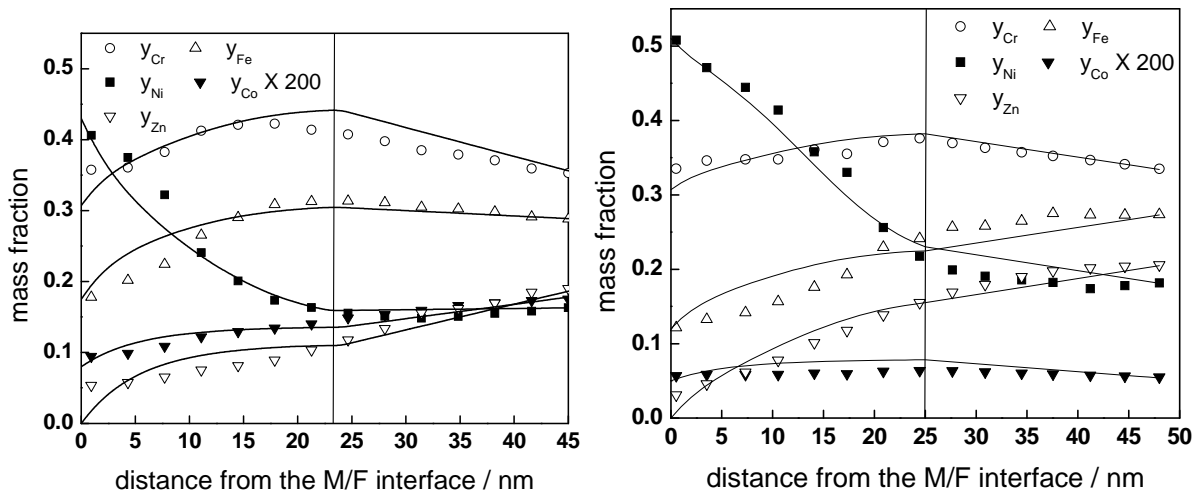

Fig. 22 *Experimental (points) and calculated (solid lines) depth profiles of the mass fractions of Fe, Cr, Ni, Co and Zn in the films formed on Alloy 690 during the first and second exposure to ca. 100 Effective Power Days in the Halden Reactor, PWR coolant conditions. The inner layer / outer layer boundary indicated with a vertical line. Experimental data taken from Refs 29-31.*
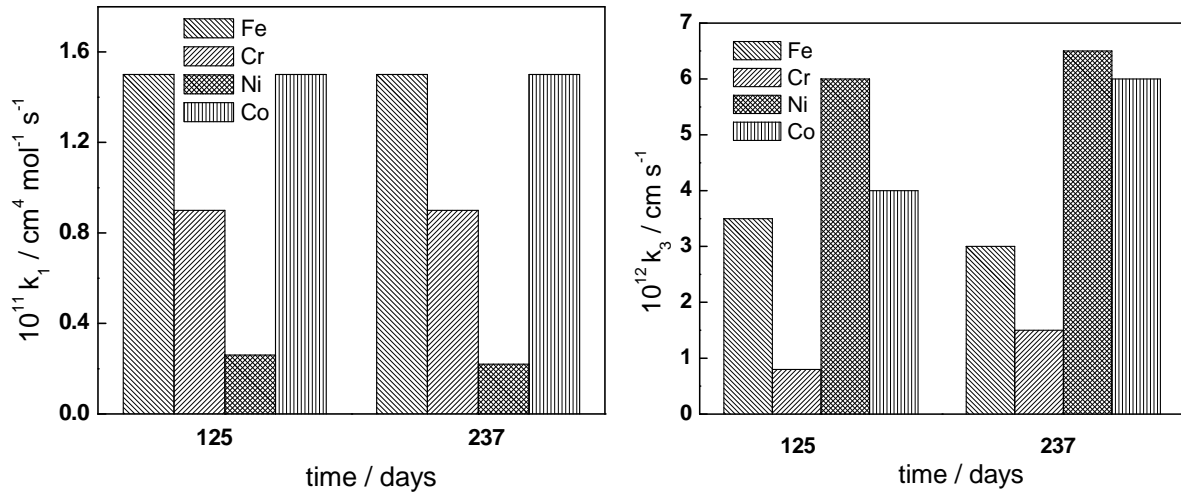
Fig. 23 *Dependence of the rate constants at the Alloy 690 / inner layer interface (left) and the inner layer/electrolyte interface (right) on the time of exposure of Alloy 690 to PWR water containing 50 ppb of Zn.*
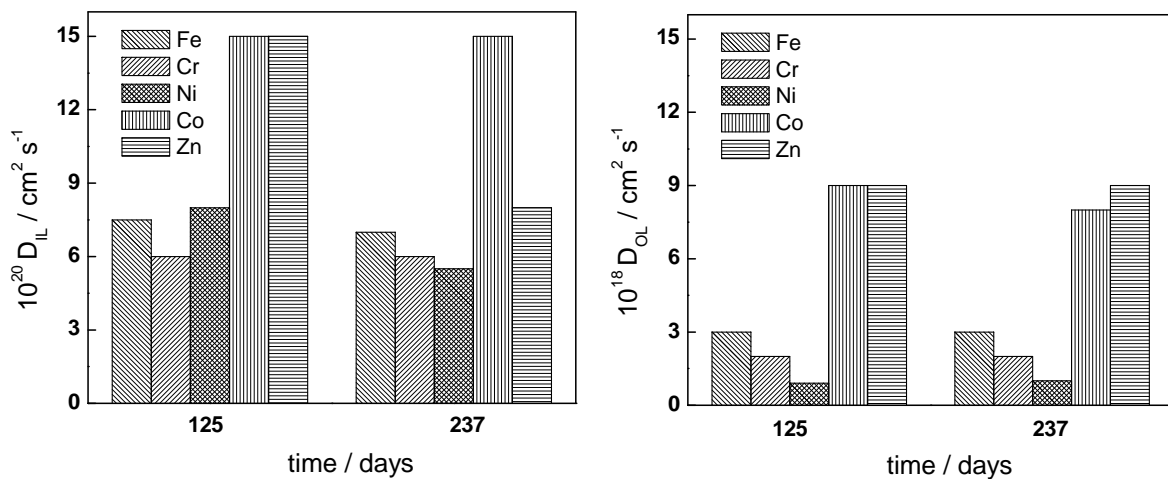

Fig. 24 *Dependence of the diffusion coefficients of inner layer constituents (left) and formal diffusion coefficients for the growth of the outer layer (right) on the time of exposure of Alloy 690 to PWR water with 50 ppb of Zn.*

A summary plot of the estimated values of the field strength in the inner layer of the oxide on Alloys 600 and 690 is given in **Fig. 25**. For short exposure times, the values of the field strength in the inner layer formed in the presence of Zn in the water are somewhat higher than those in the absence of Zn. Furthermore, a significant decrease of this parameter with time of exposure is observed. It is also worth noticing that the field strength in the inner layers on nickel-based alloys is considerably higher than that on stainless steels at short exposure times, which is in agreement with our previous calculations based on quantitative treatment of electrochemical impedance spectroscopic data [15,16]. If it is assumed that the space charge regions near grain boundaries determine the conduction through the oxide via a diffusion-migration mechanism, the decrease of the field strength in the inner layer with time of exposure can be tentatively attributed to the increase of the space charge screening length with time of exposure, which is tantamount of a decrease of the density of current carriers in the space charge regions.
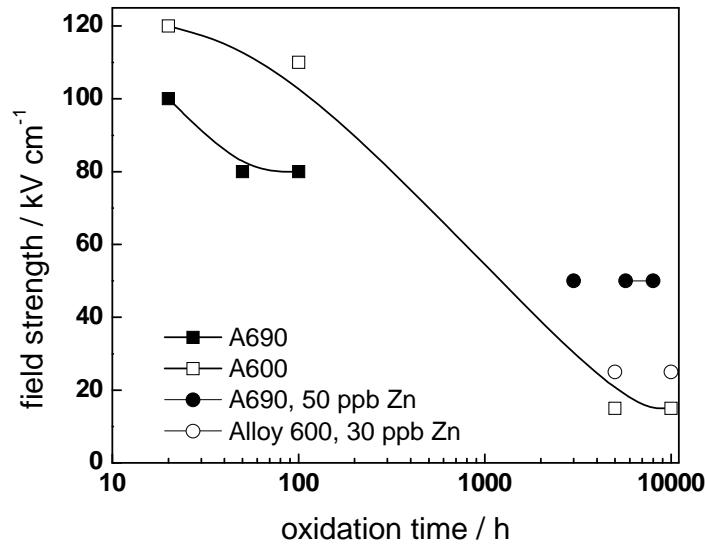
Fig. 25 *Summary of the field strength values for the inner layer on A600 and A690 calculated from the comparison of the model equations to the data in Fig. 15, Fig. 16, Fig. 17 and Fig. 22.*
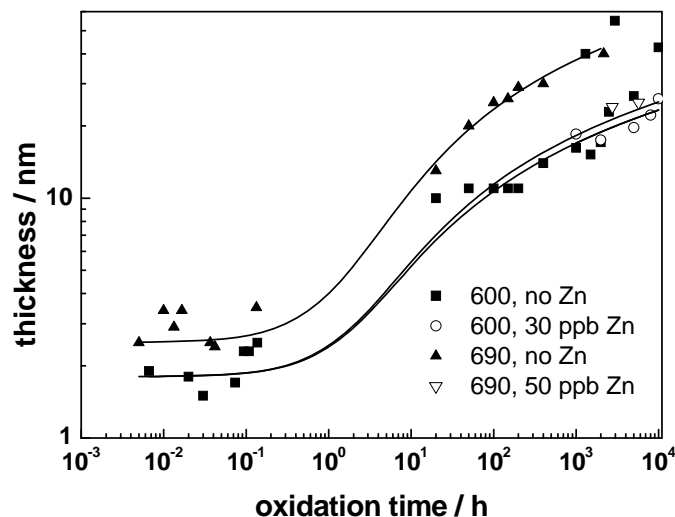

Fig. 26 *Inner layer thickness vs. time data for nickel-based alloys in simulated and in-reactor PWR water with or without Zn addition at 260-325°C (symbols) and calculated curves according to the model (solid lines).*

The inner layer thicknesses for the oxides formed on Alloys 600 and 690 in both simulated and in-reactor PWR water in the absence or presence of Zn in the water are compiled in **Fig. 26** as depending on exposure time (data from Refs. 29-31, 35-39,41,42). In the figure, the experimentally determined thickness values are compared with the thickness calculated according to equation (21). Once again a reasonable agreement is obtained without any further adjustment of parameters, which demonstrates the ability of the model to predict the kinetics of growth of the oxide on nickel-based alloys as well.

6.2 Water-Water Energy Reactor case

Fig. 27 shows Glow Discharge Optical Emission Spectroscopic (GDOES) depth profiles of the constituent elements of the oxide films on AISI 316L and 0X18H10T stainless steels exposed for 8600 h to a WWER coolant ((1200 ppm B, 15 ppm K, 15 ppm NH_3, dissolved H_2 40 $cm^3\,kg^{-1}$ STP, E_{CORR} = -0.8…-0.75 V, 250 °C) at the Loviisa 1 power plant [43].
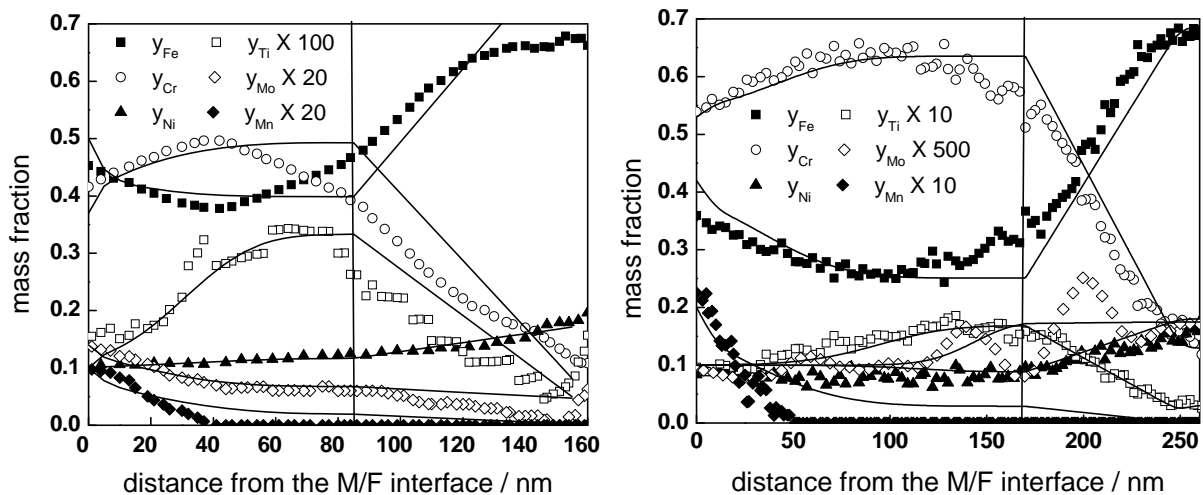

Fig. 27 Experimental (points) and calculated (solid lines) depth profiles of the mass fractions of Fe,Cr, Ni, Ti, Mo, and Mn in the films formed on AISI 316L(left) and 0X18H10T (right) after a 8600 h exposure to WWER reactor coolant at Loviisa 1 power plant. The inner layer / outer layer boundary indicated with a vertical line.

The oxides formed in WWER conditions are comparable, albeit somewhat thinner than the oxides formed in PWR conditions on compatible materials. The oxides exhibit once again a duplex structure, the inner layers being enriched in Cr and Ti and the outer layers constituted essentially of iron oxide. Despite the larger Cr content of the inner layer on 0X18H10T, its thickness is greater than that on AISI 316L which could be due to the higher Ni content of the inner layer on the latter steel acting as an additional barrier to film growth.

The calculated profiles of Fe, Cr, Ni, Ti, Mo and Mn are also shown in **Fig. 27** with solid lines and demonstrate the ability of the model to account for in-plant WWER data as well. No quantitative comparison with experimental data for Co was possible because of the relatively large scatter in the measured concentrations. Thus no kinetic and transport parameters for Co could be estimated. The estimated values of the rate constants and diffusion coefficients for the remaining constituent elements in both studied steels are collected in **Fig. 28** and **Fig. 29**, respectively. The rate constants at the inner interface values are somewhat lower than the values determined for AISI 304 in a simulated PWR coolant (**Fig. 7**-**Fig. 8**). On the other hand, the rate constants $k_{3,i}$ at the outer interface are 3-4 times larger, which could be traced to a more significant dissolution rate in the real primary coolant in comparison to the simulated one. It is worth noting that the values for both the rate constant of oxidation at the alloy/inner layer interface and dissolution at the inner layer/coolant interface for Ni are lower than those for Fe and Cr, which seems to be consistent with its oxidation state in the oxide being close to metallic, as argued by other authors as well [44]. The large values of both the rate constant at the inner layer/coolant interface and the diffusion coefficient in the inner layer for Mn are consistent with the fact that this constituent is significantly impoverished in the oxide. On the other hand, the corresponding parameters for Ti are rather low, which explains the enrichment of this component in the inner layer.
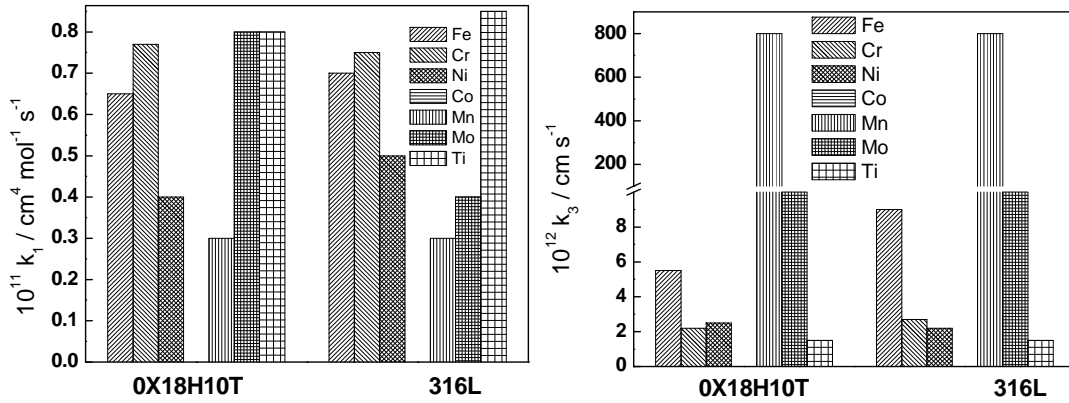
Fig. 28 Dependence of the rate constants at the steel / inner layer interface (left) and the inner layer/electrolyte interface (right) on the steel type. WWER coolant conditions.
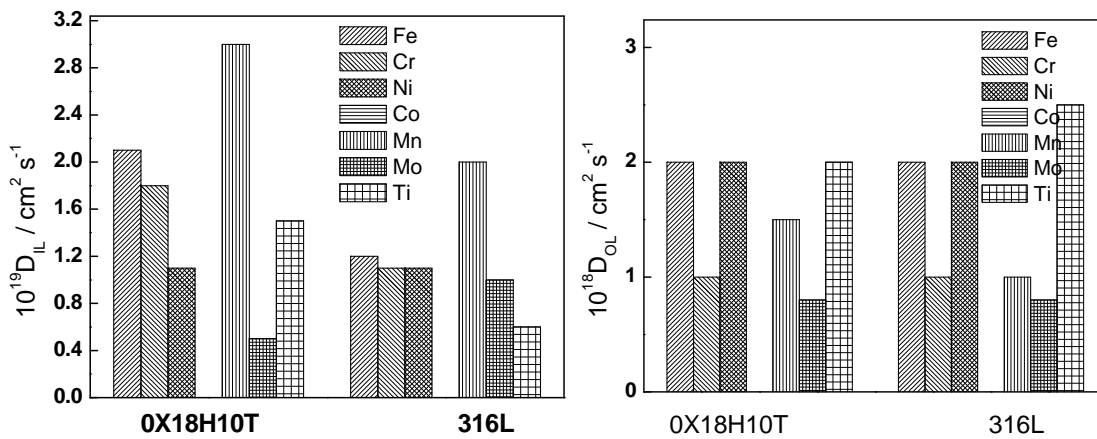

Fig. 29 Dependence of the diffusion coefficients of inner layer constituents (left) and formal diffusion coefficients for the growth of the outer layer (right) on the steel type. WWER coolant conditions.

A compilation of layer thicknesses on AISI 316 and 0X18H10T in primary WWER coolant is shown in **Fig. 30** [43-48]. Despite the limited number of experimental data available, the predictions of the proposed model can be deemed reasonable also in the WWER case.
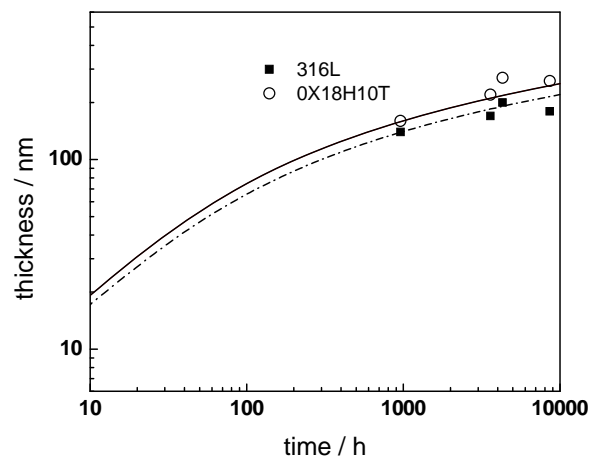

Fig. 30 A compilation of thickness vs. time data for AISI 316L and 0X18H10T as depending on the time of exposure in a primary WWER coolant. Model predictions shown with lines.

6.3 Boiling Water Reactor case

6.3.1 In-reactor exposure of stainless steels to BWR conditions

Fig. 31 shows GDOES depth profiles of the constituents of the oxide films on AISI 304 and 316 stainless steels exposed for 7200 h to a BWR coolant (conductivity less than 0.12 μScm^{-1}, dissolved oxygen 200 ppb) at the Olkiluoto 1 plant [49]. The film on AISI 304 stainless steel appears to be significantly thicker than that on AISI 316. As customary for both in-reactor and simulated BWR conditions [50-54], the films comprise an outer iron-rich layer and an inner layer containing more Cr. It is worth noting that Cr is impoverished in the films with respect to its content in the alloy substrate due to its transpassive dissolution as Cr(VI) in BWR conditions as demonstrated by wall-jet ring-disk electrode measurements [55].
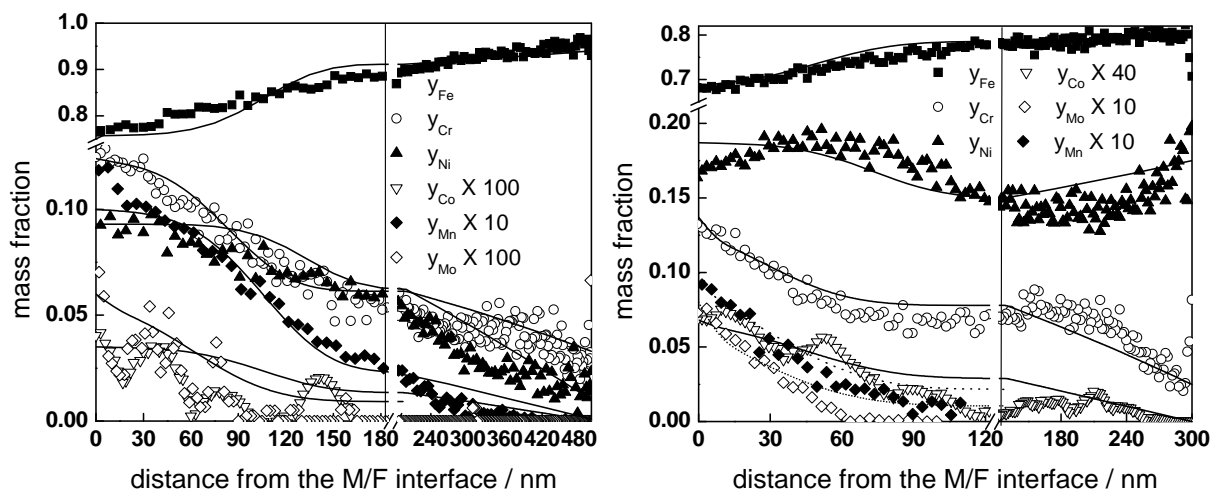

Fig. 31 *Experimental (points) and calculated (solid lines) depth profiles of the mass fractions of Fe, Cr, Ni, Mn, Mo and Co in the films formed on AISI 304(left) and AISI 316 (right) after a 7200 h exposure to BWR reactor coolant at Olkiluoto 1 power plant. The inner layer / outer layer boundary indicated with a vertical line.*

A plateau in Ni concentration is detected close to the metal / film interface in the oxide formed on AISI 304, whereas a well-pronounced maximum of Ni concentration exists in the inner layer formed on AISI 316 (**Fig. 31**). In general, it can be stated that the difference in thickness between the films formed on 304 and 316 stainless steels is largely due to the inner layer being thicker on 304 steel.

The calculated profiles of Fe, Cr, Ni and Co in the films are also shown in **Fig. 31** with solid lines and demonstrate the ability of the model to account for BWR data as well. The estimated values of the rate constants and diffusion coefficients are collected in **Fig. 32** and **Fig. 33**, respectively. The values for the rate constants and diffusion coefficients in the inner layer are rather similar for both alloys being, however, somewhat smaller for the oxide formed on AISI 316 than for that formed on AISI 304, thus explaining the lower thickness and hence the slower growth of the inner layer on the former steel. A somewhat conjectural explanation of this fact is that the more pronounced Ni-enrichment in the inner layer formed on AISI 316 acts as a diffusion barrier preventing further growth of the inner oxide on that steel. The fact that also the formal diffusion coefficients of the growth of the outer layer on AISI 316 are significantly smaller can be also explained by the larger concentration of Ni in this phase

which may hinder its growth. Indeed, the outer layer on AISI 304 is composed almost exclusively of iron (more than 90%), whereas that on AISI 316 contains ca. 15% of nickel.
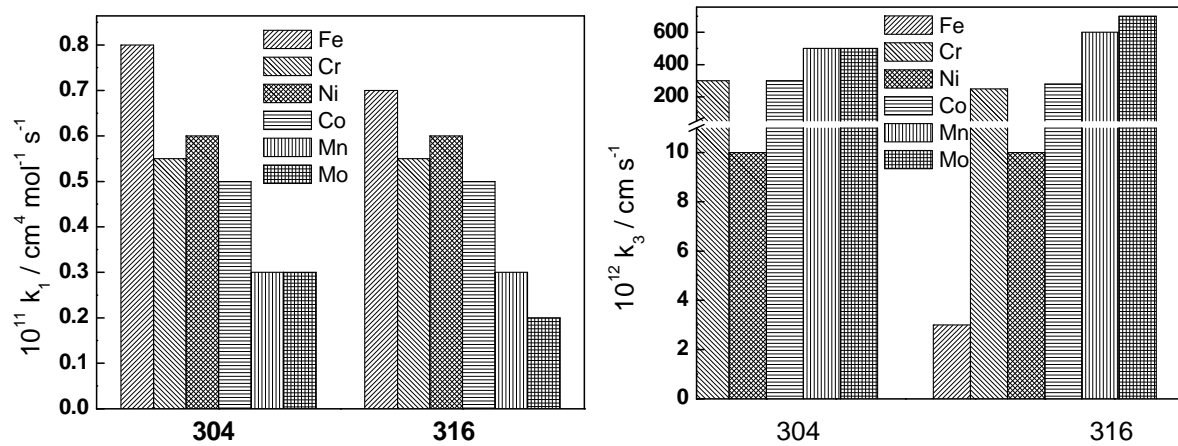

Fig. 32 Dependence of the rate constants at the steel / inner layer interface (left) and the inner layer/electrolyte interface (right) on the steel type. BWR conditions.
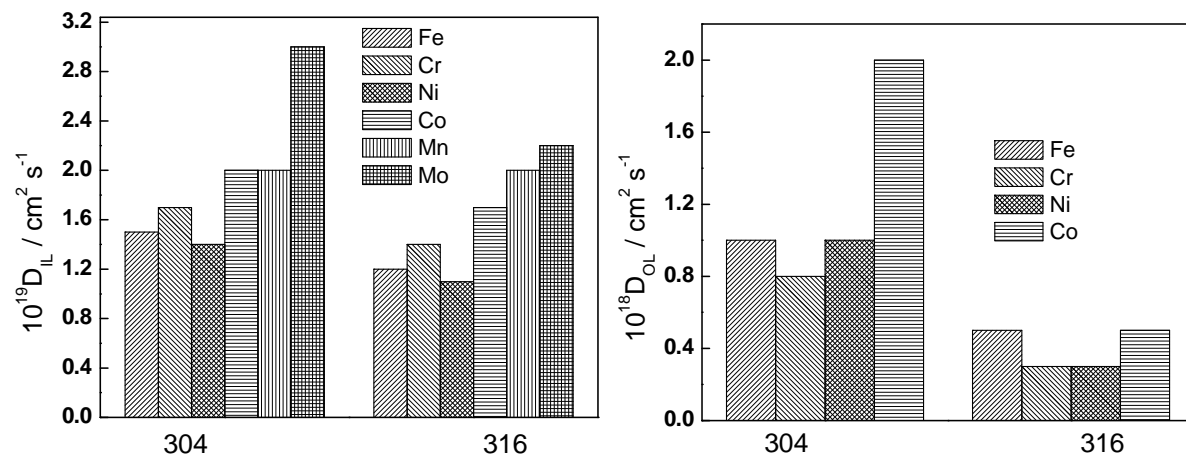

Fig. 33 Dependence of the diffusion coefficients of inner layer constituents (left) and formal diffusion coefficients for the growth of the outer layer (right) on the steel type.

On comparing the sets of parameters used to reproduce the depth profiles of AISI 304 in PWR and BWR water (e.g. **Fig. 7**-**Fig. 8** and **Fig. 32**-**Fig. 33**), it can be concluded that the most important differences are found between the rate constants at the inner layer/water interface, the diffusion coefficients in the inner layer and the formal diffusion coefficients of the growth of the outer layer. Notably, the rate constants of Cr and Co dissolution at the outer interface are orders of magnitude higher for films formed in BWR water than those for films formed in PWR water, which reflects the transpassive dissolution condition of the steels. On the basis of this result it can be tentatively assumed that Co substitutes Cr in the phase in the inner layer and is dissolved transpassively together with Cr. On the other hand, the diffusion coefficients in the inner layer are smaller in BWR water than in PWR water, which may reflect a change in the phase composition of the inner layer of oxide towards a phase containing mainly Fe(III) in which the concentration and mobility of Fe(II) interstitials is lower in comparison to those in the phase formed in PWR conditions. The fact that also the formal diffusion coefficients of the growth of the outer layer are smaller in BWR conditions could be tentatively related to the

formation of a hematite phase in this layer which growth mechanism is expected to be different from that of the spinel trevorite phase usually found in PWR water.

6.3.2 Influence of Zn on the incorporation of Co in simulated BWR conditions

This chapter focuses on the effect of ionic additions to the BWR coolant on the distribution of the main source of radiation field in BWR - radioactive cobalt - in the oxide films formed on primary loop recirculation piping [56-59]. GDOES profiles for Fe, Cr, Ni, Zn and Co in the oxide formed on AISI 304L after 1000 h of exposure to simulated BWR water containing 1 ppb of Co and different amounts of Zn [59] are shown in **Fig. 34**. In these profiles, besides the usual inner and outer layers, a third layer probably formed by deposition of foreign cations is observed. Such three-layer structures have been observed in laboratory loop experiments [60] due to the fact that saturation is achieved more readily than in real reactor conditions as flow rates are typically much smaller. Co is incorporated in both layers, but mostly in the inner layer, and its incorporation is hindered by Zn addition in analogy to the PWR results described above.

In the present context, the growth of the deposit layer has been treated in analogy to the outer layer, i.e. using the formalism described by equations (5) and (14) and defining a formal diffusion coefficient in the deposit layer. As it has been shown that also the deposit layer consists of loosely packed crystallites with electrolyte in between (see e.g. Ref. 50), a pure diffusion mechanism has been used in complete analogy to the treatment for the outer layer. The results of the calculations with such an extended version of the model are presented in **Fig. 34** with solid lines and demonstrate the ability of the approach to account for this type of data as well. The kinetic and transport parameters in the three layers used to reproduce the experimental profiles are collected in **Fig. 35** (rate constants at the interfaces) and **Fig. 36** (diffusion coefficients in the three layers and the field strength in the inner layer).
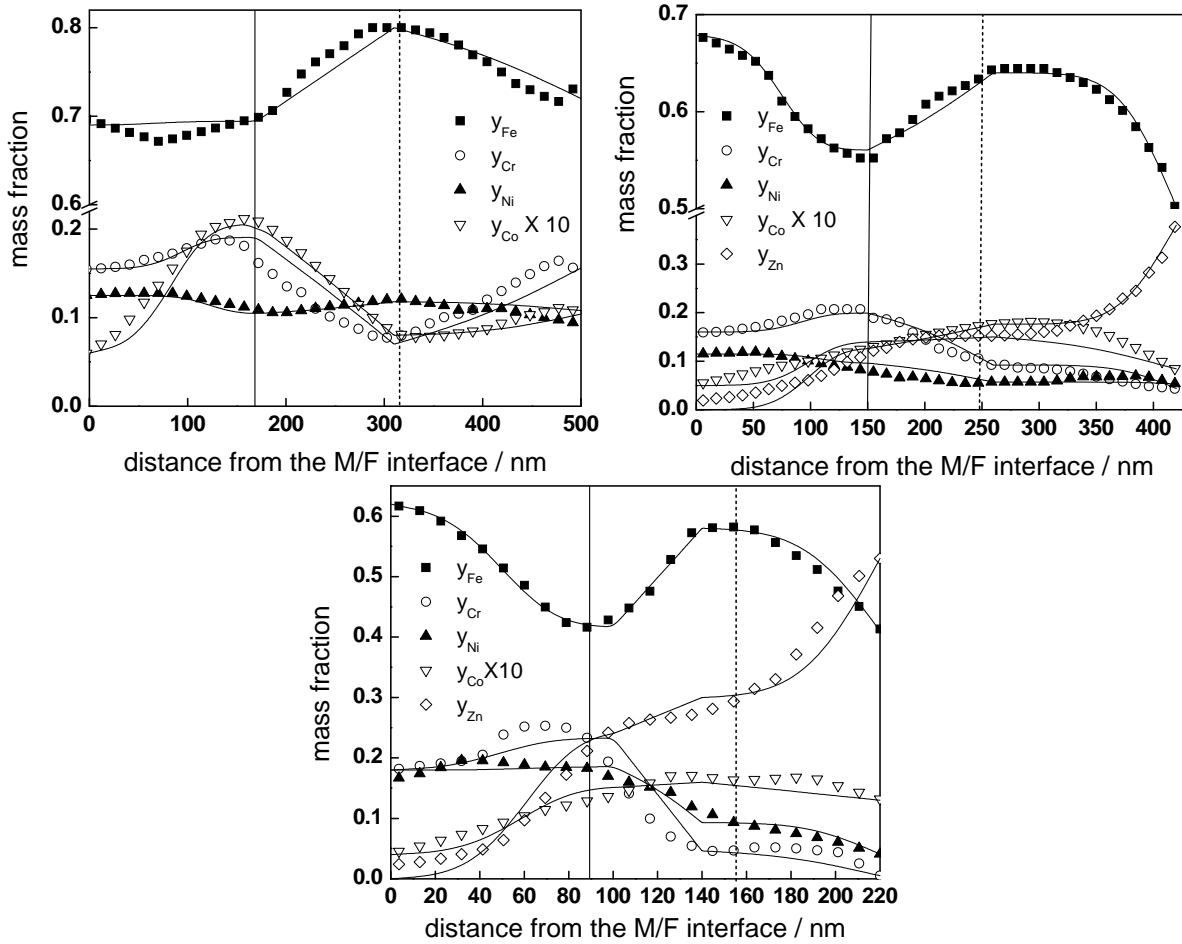
Fig. 34 *Experimental (points) and calculated (solid lines) depth profiles of the mass fractions of Fe, Cr, Ni, Co and Zn in the films formed on AISI 316 for 1000 h in simulated BWR water without Zn (above left), with 10 ppb Zn (above right) and 50 ppb Zn (below). The inner layer / outer layer and outer layer/deposited layer boundaries indicated with a vertical line. Data taken from Ref. 59.*

Fig. 35 *Dependence of the rate constants at the steel / inner layer interface (left) and the inner layer/electrolyte interface (right) on the Zn content in the simulated BWR water.*

Fig. 36 *Dependence of the diffusion coefficients in the inner layer (above, left), the formal diffusion coefficients in the outer layer (above, right) and the deposited layer (below, left) and the field strength in the inner layer (below, right), on the Zn content in the simulated BWR water.*
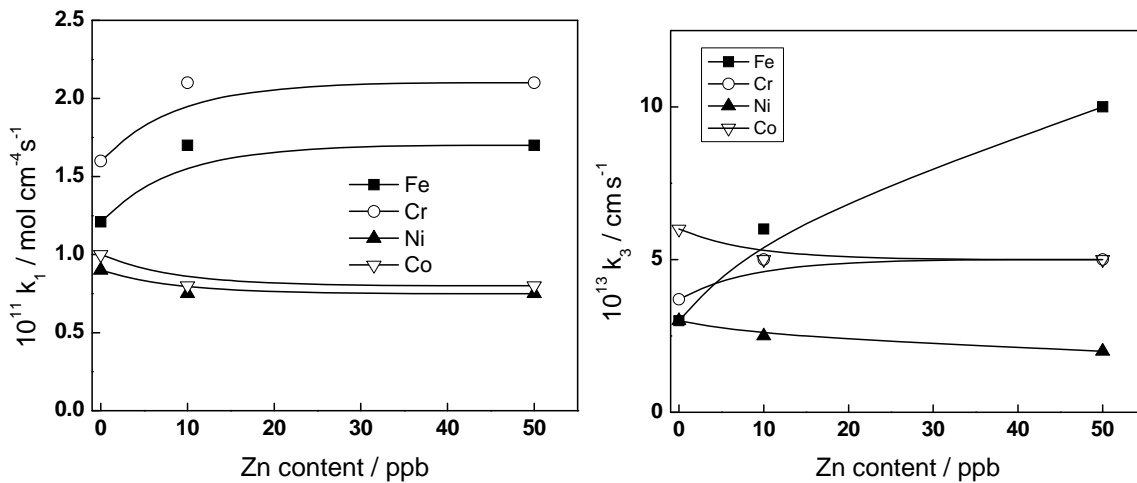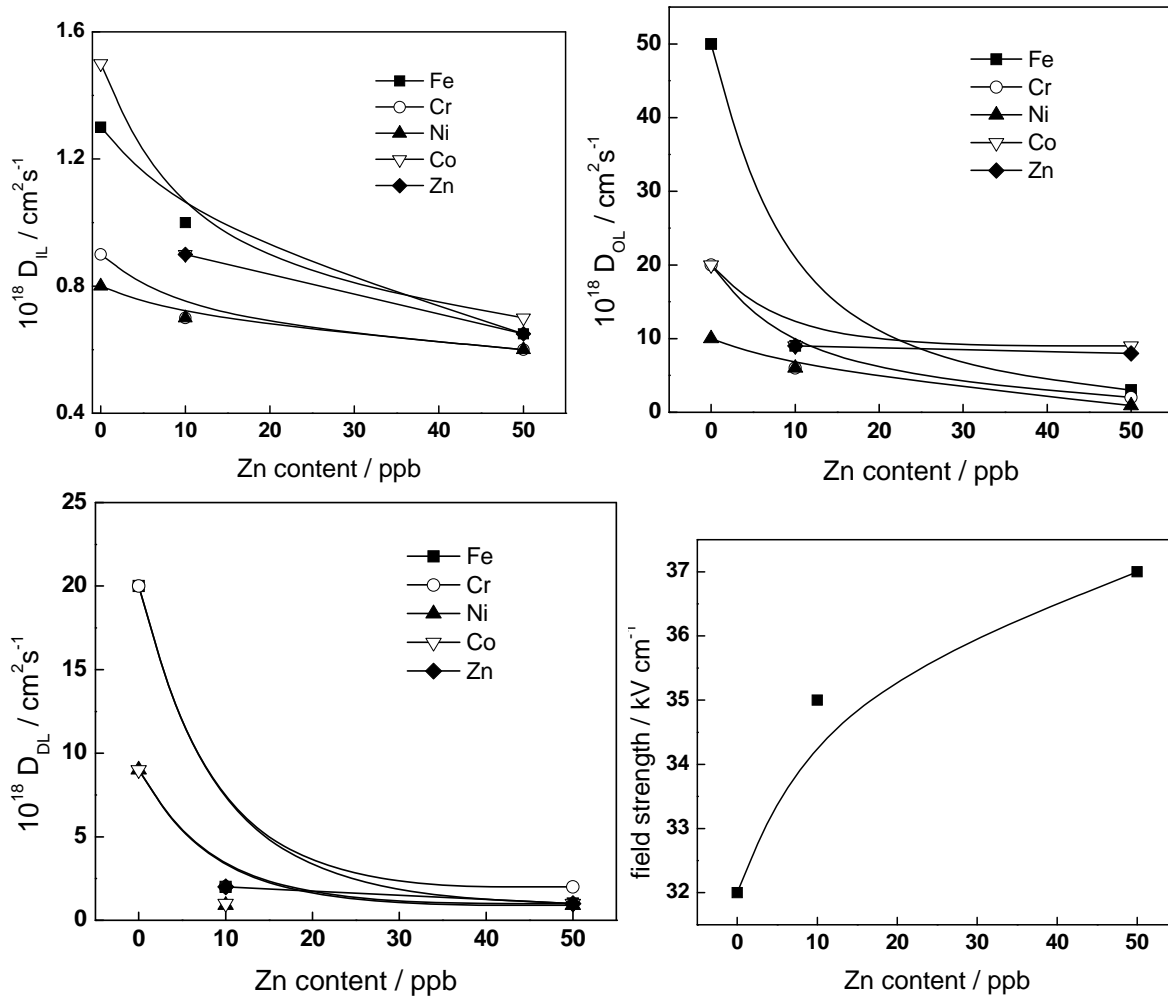
The following conclusions on the effect of Zn on the kinetic and transport parameters can be drawn on the basis of the calculatory results:

- The effect of Zn on the rate constants at the alloy/inner layer interface is small, which can be explained by the fact that Zn incorporation does not in fact reach the inner interface
- In analogy to what has been observed in PWR conditions, the incorporation of Zn in the inner layer leads to an increase of the rate constant of dissolution of Fe at the inner layer/water interface. This once more lends support to the reaction scheme of incorporation described by equations (15)-(18)
- The diffusion coefficients of constituents in the inner layer, the formal diffusion coefficients of growth of the outer and deposit layer all decrease with the increase of the Zn content in the water, the decrease being the most pronounced for the outer and deposit layers. The significant concentrations of incorporated Zn in these layers could lead to the formation of new Zn containing phases, the growth mechanism of which is different and anyway the rate of growth much slower than that of the outer and deposit layers formed in the absence of Zn.

The equilibrium constant of the exchange reaction between Zn and Fe can also be estimated from the present results using the values of the mass fractions of Zn and Fe at the inner layer/electrolyte interface (**Fig. 34**), the surface site concentration on hematite estimated earlier from titration experiments in simulated BWR water and the speciation of soluble Zn in the electrolyte calculated using literature data [61]. A value of logK = 2.8 is obtained, which lies in between the values of 5.18 and -0.23 estimated in Ref. 61 for surface complexation reactions of the type

$$2 \equiv FeOH_{1/2}^0 + Zn_{aq}^{2+} + nH_2O \rightleftarrows (\equiv FeO)_2 Zn(OH)_n^{1-n} + (n+1)H^+ \qquad (25)$$
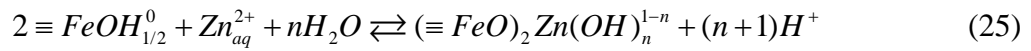
for n=2 and 5, respectively. Taking into account the fact that the experiments in Ref. 61 were performed with pure hematite in simulated BWR water, the correspondence between these two types of results is reasonable. Anyway, the equilibrium constant of Zn incorporation reaction into the oxide formed in BWR conditions is considerably (ca. 3-4 times) larger than that in PWR conditions, which could be traced to the larger equilibrium concentration of soluble Zn ions at the neutral pH of the BWR water, and also the smaller equilibrium concentration of surface sites for adsorption for the oxide formed in BWR conditions.
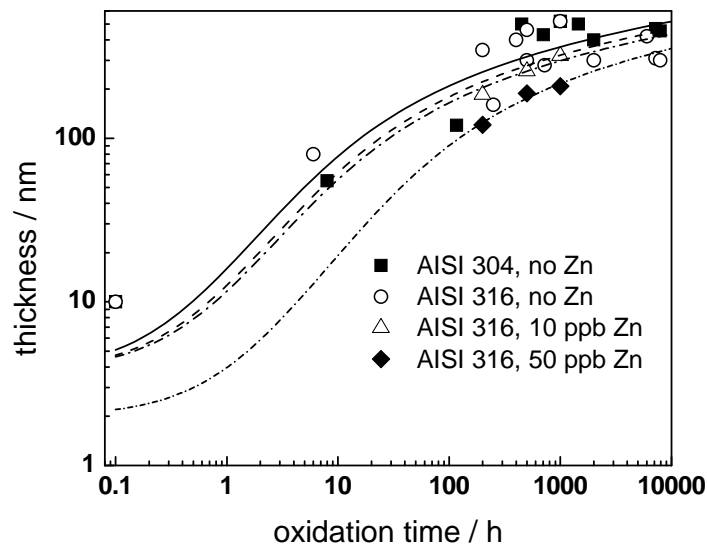
Fig. 37 A compilation of thickness vs. time data for AISI 304 and AISI 316 as depending on the time of exposure and Zn content of simulated and in-reactor BWR water. Model predictions shown with lines.

A compilation of layer thicknesses on AISI 304 and AISI 316 in simulated and in-reactor BWR coolant with or without Zn addition is shown in **Fig. 37** (data from Refs. 51-54, 59) together with the thicknesses calculated by using the estimated model parameters and equation (21). Once more a satisfactory agreement is obtained, allowing for the conclusion that the model is successful in predicting the kinetics of oxide growth also in these conditions.

7   Conclusions

Several aspects of the processes of growth and restructuring of oxide films formed on structural materials in LWRs, such as stainless steels and nickel-based alloys, have been described using the model proposed in the ANTIOXI project. The inner layer growth and

internal transport properties of charge and matter were shown to be quantitatively modelled by use of the MCM, which is developed from the solid state properties of a passive film and takes into account the coupling between transport and reaction fluxes at the interfaces, as well as ionic and electronic conduction. The interaction between the surface of the solid film and the aqueous environment has been also described in terms of incorporation of solution-originating cations and the net effects resulting from this interaction have been discussed in terms of the surface complexation approach.

The deterministic model described in the report is focused on the inner layer of oxide having an uniform composition, but also a plausible approach towards taking into account the evolution of the oxide microstructure (such as grain size and grain boundary width) on the transport of defects through the inner layer is also described. Although there are some observations that absence of a pronounced outer oxide layer will enhance the overall alloy corrosion rate, it is assumed that the overall alloy corrosion rate is limited by the rates of the net processes in this layer and can thus be explained by the MCM. The importance of the oxide film on stainless steels and nickel base materials in LWRs is, however, not limited to the formation, growth, and stability of the inner layer. In most cases, an outer oxide layer is also present. The outer layer has generally a different composition as a result of the interaction with the environment and is not considered to be part of the passivating oxide film. However, the outer layer may be important in order to prevent direct chemical attack of the protective chromium-rich layer in oxidising environments, i.e. BWRs or PWRs during shut-down. Hence, the outer layer(s) is not passivating, but can be protective. This means also that the outer layer is of fundamental importance in any effort to model the interaction between material and environment leading to activity build-up as well as to localised attack resulting in e.g. stress corrosion cracking. In the present project, a procedure to assess the kinetics of growth and hence to estimate the composition of the outer layer by using a diffusion formalism is proposed. In order to ensure the continuity of composition between the inner and outer layers, the boundary conditions at the inner layer/coolant interface in the pores of the outer layer are presumed equal to the inner boundary conditions for the outer layer. On the other hand, the boundary conditions at the interface between the coolant and the outer layer crystallites have been presumed to be fixed by thermodynamics, i.e. determined by the solubility of the individual layer constituents in the coolant water.

The outer layer is a result of the interaction of the environment with the oxide film. This interaction is of utmost importance for the modelling of the activity build-up. The pick-up and release of radioactive nuclides (and other ions) will depend on the diffusion from the outer oxide surface into the inner oxide material. The surface concentration of such species will be a function of their concentration in the water, the extent of surface complexation, and the transport rate into the inner oxide material. As yet another effect of the interaction with the environment, deposits are formed onto the outer oxide. The deposits are especially well developed in BWRs. While the outer oxide is a result of the solid state reactions in the barrier layer and within the outer layer providing a local environment controlling its formation and restructuring, the deposits are formed mainly as a result of the local bulk water chemistry conditions. This notion is shown by the very well developed rather large single crystals found on stainless steel and nickel base materials in LWR environments. In the present report, the growth of the particulate deposit layers is treated in a manner similar to that for the porous outer layer.

In reality, the interfaces between the two oxide layers and between the inner oxide film and the metal interface, as well as between the water and the outer oxide film, are mostly found to be non-uniform. The importance of an uneven water-oxide interface will be small due to the

very fast relative diffusion rates in water at elevated temperatures with regard to the dimensions of the oxide films. Similarly, the uneven oxide film appearance will have no importance for the modelling of the impact of the deposited crystals for the same reason. The importance of an uneven inner layer could be of more importance. However, in reality a slightly thicker oxide layer would constitute a more pronounced transport barrier and a variation in this thickness would be self-regulating to result in a barrier layer oxide of similar transport limiting properties for all areas of similar local conditions on similar materials. An important step in going from an idealised oxide model of a uniform and even oxide film to the real oxide would be the introduction of porosity instead of using the formal approach to the growth and restructuring of the outer and deposit layers as outlined in the present chapter.

8   Summary

An integrated deterministic model for corrosion and activity incorporation in oxides on structural materials in nuclear power plant coolant circuits is proposed based on fundamental physico-chemical mechanisms. In order to ensure adequate modelling, uncertain or non-determined fundamental parameters are set or adjusted within the range of reasonable values by evaluating well-defined or well-controlled in-plant observations or laboratory experiments. As a result of the calculation procedure developed on the basis of the model, the kinetic and transport parameters of the growth and restructuring of the oxides on austenitic stainless steels (AISI 304, 0X18H10T and AISI 316) and nickel based alloys (Alloys 600 and 690) in Light Water Reactors (LWRs) were determined via quantitative comparison of the equations of the Mixed-Conduction Model for oxide films with ex-situ analytical results on thickness and composition of such layers obtained from both laboratory and in-reactor exposures. The obtained parameters were used to predict general corrosion of stainless alloys in terms of oxide film growth and restructuring, as well as corrosion release in several specific cases covering all the three types of LWRs – Boiling Water Reactors (BWRs), Pressurised Water Reactors (PWRs) and Water-Water Energy Reactors (WWERs). Kinetic and transport parameters for the incorporation of Co and Zn in the oxide layers on stainless steels and nickel alloys are also estimated by reproducing the experimental depth profiles of these elements. The diffusion-migration equations for the non-steady state transport of such species were solved subject to the boundary conditions at the solution side set by the stability constants of the corresponding Zn and Co complexes. The calculatory results are discussed in terms of the influence of incorporation of solution-originating species on the kinetics of film growth and layer restructuring.

9   List of symbols

D_{Co}	diffusion coefficient of Co in the inner layer, $cm^2 s^{-1}$
$D_{Co,OL}$	formal diffusion coefficient of Co in the outer layer, $cm^2 s^{-1}$
D_{Cr}	diffusion coefficient of Cr in the inner layer, $cm^2 s^{-1}$
$D_{Cr,OL}$	formal diffusion coefficient of Cr in the outer layer, $cm^2 s^{-1}$
D_{Fe}	diffusion coefficient of Fe in the inner layer, $cm^2 s^{-1}$
$D_{Fe,OL}$	formal diffusion coefficient of Fe in the outer layer, $cm^2 s^{-1}$
D_{Ni}	diffusion coefficient of Ni in the inner layer, $cm^2 s^{-1}$
$D_{Ni,OL}$	formal diffusion coefficient of Ni in the outer layer, $cm^2 s^{-1}$
D_{Zn}	diffusion coefficient of Zn in the inner layer, $cm^2 s^{-1}$
$D_{Zn,OL}$	formal diffusion coefficient of Zn in the outer layer, $cm^2 s^{-1}$
$\vec{E}$	field strength in the inner layer, $V\ cm^{-1}$
F	Faraday number, $96487\ C\ mol^{-1}$
K	equilibrium constant of surface complexation reactions
$K_{enr,Co,i}$	enrichment factor of Co at the inner layer/ coolant interface
$K_{enr,Zn,i}$	enrichment factor of Zn at the inner layer/ coolant interface
$K_{enr,Zn,o}$	enrichment factor of Zn at the outer layer/coolant interface
$k_{1,Cr}$	rate constant of oxidation of Cr at the alloy/inner layer interface, $cm^4 mol^{-1} s^{-1}$
$k_{1,Fe}$	rate constant of oxidation of Fe at the alloy/inner layer interface, $cm^4 mol^{-1} s^{-1}$
$k_{1,Ni}$	rate constant of oxidation of Ni at the alloy/inner layer interface, $cm^4 mol^{-1} s^{-1}$
$k_{3,Cr}$	rate constant of dissolution of Cr at the inner layer/ coolant interface, $cm\ s^{-1}$
$k_{3,Fe}$	rate constant of oxidation of Fe at the inner layer/ coolant interface, $cm\ s^{-1}$
$k_{3,Ni}$	rate constant of oxidation of Ni at the inner layer/ coolant interface, $cm\ s^{-1}$
L_i	inner layer thickness, cm
$L(t=0)$	initial film thickness, cm
L_o	outer layer thickness, cm
R	universal gas constant, $8.314\ J\ mol^{-1}\ K^{-1}$
T	temperature, K
$V_{m,MO}$	molar volume of the phase in the inner layer, $cm^3 mol^{-1}$
X	formal valency state of Fe in the inner layer
y_{Co}	mass fraction of Co in the oxide
y_{Cr}	mass fraction of Cr in the oxide
y_{Fe}	mass fraction of Fe in the oxide
y_{Ni}	mass fraction of Ni in the oxide
y_{Zn}	mass fraction of Zn in the oxide
$y_{Co,a}$	mass fraction of Co in the alloy substrate
$y_{Cr,a}$	mass fraction of Cr in the alloy substrate
$y_{Fe,a}$	mass fraction of Fe in the alloy substrate
$y_{Ni,a}$	mass fraction of Ni in the alloy substrate
$y_{Zn,a}$	mass fraction of Zn in the alloy substrate
α_1	transfer coefficient of the oxidation reaction at the alloy/inner layer interface
ε	dielectric constant of the oxide
ε_0	dielectric permittivity of vacuum, $8.85 \times 10^{-14}\ F\ cm^{-1}$
ψ	electrostatic potential, V

References

1. Chao, C.Y.; Lin, L.F.; Macdonald D.D. *J. Electrochem. Soc.* 1981, *128*, 1187-1194.
2. Macdonald, D.D. *J. Electrochem Soc.* 1992, *139*, 3434-3442.
3. Macdonald, D.D. *Pure Appl. Chem.* 1999, *71*, 951-978.
4. Macdonald, D.D.*J. Electrochem. Soc.* 2006, *153,* B213-B224.
5. Fromhold Jr., A.T.; Cook, E. L. *J. Appl. Phys.* 1967, *38*, 1546-1553.
6. Young, L.*Trans. Faraday Soc.* 1955, *51*, 1250-1255.
7. Cahan, B.D.; Chen, C.-T. *J. Electrochem. Soc.* 1982, *129*, 921-925.
8. Bojinov, M.; Fabricius, G.; Laitinen, T.; Mäkela, K.; Saario, T.; Sundholm, G. *J. Electrochem. Soc.* 1999, *146*, 3238-3247.
9. Bojinov, M.; Fabricius, G.; Laitinen, T.; Mäkela, K.; Saario, T.; Sundholm, G. *Electrochim. Acta* 2000, *45*, 2029-2048.
10. Bojinov, M.; Fabricius, G.; Laitinen, T.; Mäkela, K.; Saario, T.; Sundholm, G. *Electrochim. Acta* 2001, *46*, 1339-1358.
11. Bojinov, M.; Fabricius, G.; Kinnunen, P.Laitinen, T.; Mäkela, K.; Saario, T.; Sundholm, G. *J. Electroanal. Chem.* 2001, *504*, 29-44.
12. Beverskog, B.; Bojinov, M.; Kinnunen, P.; Laitinen, T.; Mäkelä, K.; Saario, T. *Corros. Sci.* 2002, *44*, 1923-1940.
13. Bojinov, M.; Kinnunen, P.; Sundholm, G. *Corrosion* 2003, *59*, 91-103.
14. Betova, I.; Bojinov, M.; Kinnunen, P.; Mäkelä, K.; Saario, T. J. Electroanal. Chem. *2004*, *572*, 211-223.
15. Bojinov, M.; Kinnunen, P.; Lundgren, K.; Wikmark, G. *J. Electrochem. Soc.* 2005, *152*, B250-B261.
16. Bojinov, M.; Galtayries, A.; Kinnunen, P.; Machet, A.; Marcus, P. *Electrochim. Acta* 2007, *52*, 7475-7483.
17. Betova, I.; Bojinov, M.; Kinnunen, P.; Lundgren, K.; Saario, T. *J. Electrochem. Soc.* 2008, *155*, C81-C92.
18. Zhang L.; Macdonald, D.D. *Electrochim. Acta* 1998, *43,* 2673-2685.
19. Tiedemann, W.; Newman, J. *J. Electrochem. Soc.* 1972, *119*, 186-188.
20. Lundgren, K.; Kelen, T.; Gunnarsson, M.; Ahlberg, E. *Proceedings of CHIMIE 2002*, *La chimie de l'eau dans les réacteurs nucléaires -Optimisation de l'exploitation et développements nouveaux*, SFEN, Avignon, France, 2002.
21. Betova, I., Bojinov, M., Kinnunen, P., Lehikoinen, J., Lundgren, K., Saario, T. *Proceedings of ICAPP'07*, SFEN, Avignon, France, 2008, paper No. 7122.
22. Beverskog, B.; Puigdomenech, I. *Corrosion,* 1999, *55*, 1077-1087.
23. Ziemniak, S.E.; Hanson, M. *Corros. Sci.* 2002, *44*, 2209-2230.
24. Ziemniak, S.E.; Hanson, M. *Corros. Sci.* 2006, *48*, 2525-2546.
25. Lister, D.H.; Venkateswaran, G. *Nucl. Technol.* 1999, *125*, 316-331.
26. Beverskog, B. *Proc. International Conference Water Chemistry of Nuclear Reactor Systems*, American Nuclear Society, San Francisco, CA, 2004, paper 2.7.
27. Bojinov, M.; Kinnunen, P.; Olin, M. VTT-R-10851-07, VTT Technical Research Centre of Finland, Espoo, 2008.
28. Barale, M., Mansour, C., Carrette, F., Pavageau, E.M., Catalette, H., Lefèvre, G., Fedoroff, M., Cote, G., *J. Nucl. Mater.* 2008, *381*, 302-308.
29. Bennett, P.J.: Gunnerud, P.; Petersen, J.K.; Harper, A. *Water Chemistry of Nuclear Reactor Systems 7*, British Nuclear Energy Society, London, 1996; Vol.1, pp. 189-193.
30. Bennett, P.J.: Gunnerud, P.; Loner, J.; Petersen, J.K.; Harper, A. *Water Chemistry of Nuclear Reactor Systems 7*, British Nuclear Energy Society, London, 1996; Vol.1, pp. 293-296.

31. Beverskog, B.; Mäkelä, K. *Proc.of the JAIF International Conference on Water Chemistry in Nuclear Power Plants*, Japanese Nuclear Society, Kashiwazaki, Japan, 1998, p. 89-98.

32. Szklarska-Smialowska, Z.; Chou, K.; Xia, Z. *Corros. Sci.* 1992, *32*, 609-619.

33. Tapping, R.L.; Davidson, R.D.; McAlpine, E.; Lister, D.H. *Corros. Sci.* 1986, *26*, 563-576.

34. Lister, D.H.; McAlpine, E.; Davidson, R.D. *Corros. Sci.* 1987, *27*, 113-140.

35. Machet, A. *Etude des premiers stades d'oxydation d'alliages inoxydables dans l'eau à haute température*, PhD Thesis, Université Pierre et Marie Curie (Paris VI), Paris, 2004.

36. Machet, A.; Galtayries, A.; Marcus, P.; Combrade, P.; Jolivet. P.; Scott, P. *Surf. Interf. Anal.* 2002, *34,* 197-200.

37. Machet, A.; Galtayries, A.; Zanna, S.; Klein, L.; Maurice, V.; Jolivet. P.; Foucault, M.; Combrade, P.; Scott, P.; Marcus, P. *Electrochim. Acta* 2004, *49*, 3957-3964.

38. Ziemniak, S.E.; Hanson, M. *Corros. Sci.* 2006, *48*, 498-521.

39. Ziemniak, S.E.; Hanson, M. *Corros. Sci.* 2006, *48*, 3330-3348.

40. Chevalier, S.; Desserey, F.; Larpin, J.P. *Oxid. Met.* 2005, *64*, 219-234.

41. Carette, F.; Lafont, M.C.; Chatainier, G.; Guinard, L.; Pieraggi, B. *Surf. Interf. Anal.* 2002, *34*, 135-138.

42. Delabrouille, F.; Viguier, B.; Legras, L.; Andrieu, E. *Mater. High Temp.* 2005, *22*, 287-292.

43. Bojinov, M.; Kinnunen, P.; Kukkonen, A.; Laitinen, T.; Mäkela, K.; Saario, T.; Sirkiä, P. *Plant Life Management. Progress for structural integrity,* Solin, J.; Ed.; VTT Symposium 227, VTT Technical Research Centre of Finland, Espoo, 2003, pp. 137-151.

44. Schuster, E.; Neeb, H.; Ahlfänger, W.; Henkelmann, R.; Järnström, R.T. *J. Nucl. Mater.* 1988, *152*, 1-8.

45. Bojinov, M.; Ehrnsten, U.; Kinnunen, P.; Laitinen, T.; Mäkela, K.; Saario, T.; Sirkiä, P.; Taivalaho, L.; Buddas, T.; Halin, M.; Tompuri, K. *Plant Life Management. Midterm Status of an R&D Project.* Solin, J.; Ed.; VTT Symposium 218, VTT Technical Research Centre of Finland, Espoo, 2002, pp. 211-240.

46. Zmitko, M.; Svarc, V.; Hanus, V.; Janesik, J.; Marcinsky, P.; Grygar, T. *Proceedings of Chimie 2002, International Conference Water Chemistry in Nuclear Reactor Systems. Operation Optimisation and New Developments*, Avignon, France, SFEN, French Nuclear Energy Society (2002).

47. Grygar, T.; Zmitko, M. *Proceedings of Chimie 2002, International Conference Water Chemistry in Nuclear Reactor Systems. Operation Optimisation and New Developments,* Avignon, France, SFEN, French Nuclear Energy Society (2002).

48. Zmitko, M. *Proc. 14th International Conference on the Properties of Water and Steam,* Kyoto, Japan, 2005, pp. 539-544.

49. Bojinov, M.; Kinnunen, P.; Laitinen, T.; Mäkela, K.; Saario, T.; Sirkiä, P. *Plant Life Management. Progress for structural integrity,* Solin, J.; Ed.; VTT Symposium 227, VTT Technical Research Centre of Finland, Espoo, 2003, pp. 123-136.

50. Kim, Y.-J. *Corrosion* 1995, *51*, 849-860.

51. Degueldre, C.; O'Prey, S.; Francioni, W. *Corros. Sci.* 1996, *38*, 1763-1782.

52. Degueldre, C.; Buckley, D.; Dran, J.C.; Schenker, E. *J. Nucl. Mater.* 1998, *252*, 22-27.

53. Hemmi, Y.; Uruma, Y.; Ichikawa, N. *J. Nucl. Sci. Technol.* 1994, *31*, 443-455.

54. Wambach, J.; Wokaun, A.; Hiltpold, A. *Surf. Interface Anal.* 2002, *34*, 164-170.

55. Bojinov, M.; Kinnunen, P.; Laitinen, T.; Mäkelä, K.; Mäkelä, M.; Saario, T.; Sirkiä, P. *Corrosion* 2001, *57*, 387-393.

56. Ono, S.; Naginuma, M.; Kumagai, M.; Kitamura, M.; Tachibana, K.; Ishigure, K. *J. Nucl. Sci. Technol.* 1995, *32*, 125-132.

57. Honda, T.; Ohashi, K.; Furutani, Y.; Minato, A. *Corrosion* 1987, *43*, 564-570.

58. Hosokawa, H.; Uetake, N.; Ushida, K.; Nakamura, M.; Mochizuki, K.; Nagata, T.; Ogawa, N.; Baba, T.; Ono, S.; Ishigure, K. *Proceedings of CHIMIE 2002*, *La chimie de l'eau dans les réacteurs nucléaires -Optimisation de l'exploitation et développements nouveaux*, SFEN, Avignon, France, 2002, paper 136.

59. Inagaki, H.; Nishikawa, A.; Sugita, Y.; Tsuji, T. *J. Nucl. Sci. Technol.* 2003, *40*, 143-152.

60. Betova, I.; Bojinov, M.; Helin, M.; Laitinen, T.; Muttilainen, E.; Mäkelä, K.; Reinvall, A.; Sirkiä, P. *Proceedings of the International Conference Water Chemistry of Nuclear Reactor Systems*, San Francisco, CA, October 10-14, 2004, pp. 282-288.

61. Kinnunen, P.; Bojinov, M.; Lehikoinen, J.; Lundgren, K. *SAFIR, The Finnish Research Programme on Nuclear Power Plant Safety 2003– 2006, Final Report,* Karita-Puska, E.; Ed.; VTT Research Notes 2363, V TT Technical Research Centre of Finland, Espoo, 2006, pp.115-121.